Mathematics **2014**, *1*, 136-171; doi:10.3390/math2030136

OPEN ACCESS

mathematics

ISSN 2227-7390

www.mdpi.com/journal/mathematics

Article

Modeling the Influence of Environment and Intervention on Cholera in Haiti

Stephen Tennenbaum *, Caroline Freitag and Svetlana Roudenko

Department of Mathematics, The George Washington University, 2115 G St. NW, Washington, DC 20052, USA; E-Mails: calliefreitag@gmail.com (C.F.); roudenko@gwu.edu (S.R.)

* Author to whom correspondence should be addressed; E-Mail: set1@gwu.edu; Tel.: +1-202-994-6235.

Received: 12 April 2014; in revised form: 24 May 2014 / Accepted: 15 August 2014 / Published: 5 September 2014

Abstract: We propose a simple model with two infective classes in order to model the cholera epidemic in Haiti. We include the impact of environmental events (rainfall, temperature and tidal range) on the epidemic in the Artibonite and Ouest regions by introducing terms in the transmission rate that vary with environmental conditions. We fit the model on weekly data from the beginning of the epidemic until December 2013, including the vaccination programs that were recently undertaken in the Ouest and Artibonite regions. We then modified these projections excluding vaccination to assess the programs' effectiveness. Using real-time daily rainfall, we found lag times between precipitation events and new cases that range from 3.4 to 8.4 weeks in Artibonite and 5.1 to 7.4 in Ouest. In addition, it appears that, in the Ouest region, tidal influences play a significant role in the dynamics of the disease. Intervention efforts of all types have reduced case numbers in both regions; however, persistent outbreaks continue. In Ouest, where the population at risk seems particularly besieged and the overall population is larger, vaccination efforts seem to be taking hold more slowly than in Artibonite, where a smaller core population was vaccinated. The models including the vaccination programs predicted that a year and six months later, the mean number of cases in Artibonite would be reduced by about two thousand cases, and in Ouest by twenty four hundred cases below that predicted by the models without vaccination. We also found that vaccination is best when done in the early spring, and as early as possible in the epidemic. Comparing vaccination between the first spring and the second, there is a drop of about 40% in the case reduction due to the vaccine and about 10% per year after that.

Keywords: cholera; Haiti; tides; precipitation; epidemic model; vaccination

1. Introduction

On 12 January 12 2010, a 7.0 magnitude earthquake struck near Haiti's capital, Port-au-Prince [1]. The poorest nation in the Western Hemisphere, the earthquake shattered Haiti's already weak infrastructure [1]. Thousands of Haitians were killed, and even more were forced to flee to resettlement camps [1].

In October 2010, the first case of cholera, ever on record, was reported in Haiti. A later UN investigation revealed the specific strain of *V. cholerae* came from South Asia [2]. The UN investigation and epidemiological literature suggest that the epidemic began outside of a UN peacekeeper camp near Mirebalais in the Centre department, along the Artibonite River [2,3]. As *V. cholerae* is a waterborne pathogen, the Artibonite River is the ostensible route through which the disease spread throughout Haiti's ten administrative regions, called departments [4].

Anecdotal news reports describe the dismal situation for thousands of Haitians that still remain displaced months after the earthquake. Sewage of millions of people flow through open ditches. Human waste from septic pits and latrines is dumped into the canals and, after it rains, ends up in the sea. Those living close to the water use over-the-sea toilets, and next to these outhouses, fishing boats unload and sell the fish from plastic buckets, *etc*. [5].

Haiti's two most populous regions, Ouest and Artibonite, were also the two regions hardest hit by the epidemic. Cases in Ouest and Artibonite account for 60% of the total burden of cholera in Haiti [6]. For this reason, we chose to focus our analysis on the Ouest and Artibonite regions. By 7 April 2012, cholera had affected 5.7% of the total population in Ouest and 6.9% of the population in Artibonite [6] (note: population data for Haiti is from 2009 [4], one year before the earthquake).

1.1. Previous Research

Previous models dealing with cholera and climatic conditions (rainfall, precipitation and tides) in Haiti vary widely in approach. There are a number of dynamical models using variations of SIWR (Susceptible, Infected, contaminated Water, Recovered), proposed in 2001 by Codeço [7] and, later, Tien and Earn [8], that address the situation in Haiti [9–11]. These models look at various compartmental and spatial structures, but do not take environmental conditions explicitly into account. The models proposed by Tuite, *et al*. [11] and Bertuzzo, *et al*. [10], for example, both incorporated a "gravity" term to study the interaction among departments. The model proposed by Andrews and Basu [9] accounted for a bacterial "hyperinfectivity" stage, following research by Hartley, *et al*. in 2006 showing that *V. cholerae* initially has a higher infectivity before it decays to a lower infective rate in the aquatic reservoir. A paper by Chao *et al*. [12] uses an agent-based model to investigate hypothetical vaccination programs in Haiti. This model examined various vaccination strategies that included pre-vaccination and early (21 days after the epidemic begins) reactive vaccination using various strategies.

Other papers [13–15] do take precipitation directly into account in cholera. The first [13] is a spatiotemporal Markov chain model using seasonal rainfall that drives disease outbreaks in an urban core, which then propagates to other areas of the city. The second [14] deals specifically with Haiti and was done by the same group that produced one of the earlier papers [10]. In [14], they looked at the reliability of the earlier studies, and they found that although those models do well in capturing the early dynamics of the epidemic, they fail to track latter recurrences forced by seasonal patterns [14]. As a follow up, Rinaldo *et al.* [14] add a precipitation forcing function to their original model along with other modifications, such as the river network and population mobility. These modifications produce a better fit to the observed pattern of cases over the first year of the epidemic. The third model by Eisenberg *et al.* [15] looks at the link between precipitation and disease outbreaks in Haiti from a statistical and dynamical modeling approach. Their dynamical system is a hybrid SIWR-SIR approach, where the infection rate of the SIWR component includes a rainfall forcing function and the infection rate of the SIR component accounts for short-term direct contacts with infected individuals.

In addition, these models assessed the impact of potential intervention strategies, including vaccination. Bertuzzo found that a vaccination campaign aiming to vaccinate 150,000 people after 1 January 2011, would have little effect, in part because of the late timing and in part because of the large proportion of asymptomatic individuals who would need to get vaccinated [10]. Both the models proposed by Tuite, *et al.* [11] and Andrews and Basu [9] suggest that vaccination campaigns would have a modest effect. In March 2012, Partners in Health began vaccinating 100,000 individuals with Shanchol, a two-dose cholera vaccine [16]. The size of the campaign was limited by the size of the global stockpile of Shanchol [16]. The vaccination campaign is targeted at 50,000 individuals living in the slums of Port-au-Prince (Ouest region), where population density is thought to increase the rate of cholera exposure, and at 50,000 individuals living in the Artibonite River valley (Artibonite region), where the epidemic began [16]. Chao *et al.* [12] showed that a targeted vaccination strategy would have the best results for this limited supply of vaccine, and by early vaccinating 30% of the population and hygienic improvements, the cases could be reduced by as much as 55%.

In 2001, Codeço proposed introducing an oscillating term to model seasonal variability [7]. However, none of the Haiti-specific models published prior to 2012 account for seasonality. Haiti experienced flooding in June 2011, October 2011, and March 2012 [17]. As cholera reached an endemic state in Haiti, connecting precipitation explicitly to disease dynamics became more suitable. Mathematical models incorporated seasonality in order to more accurately predict the course of the epidemic and to simulate the effects of potential interventions. In April 2012, Rinaldo *et al.* [14] reexamined the above four models (including their own [10]) and concluded that, among other factors, seasonal rainfall patterns were necessary to account for resurgences in the epidemic. They use long-term monthly averages to augment the bacterial growth term of contaminated water-bodies. Eisenberg *et al.* [15] examined rainfall patterns and assessed lag times between precipitation events and cases in the early epidemic. These indicated short delays of four to seven days. Other papers dealing with environmental factors were: (1) a study of cholera in Zanzibar, East Africa that demonstrated an eight-week fixed delay [18] between rainfall and cholera outbreaks; and (2) a study in Bangladesh [19] that reports a somewhat shorter delay (four weeks). Both of these studies use a statistical approach with seasonal data. Both also made note of the potential influence of ocean environmental factors, and the Reyburn *et al.* paper

included sea surface height and sea surface temperature in their analysis, but failed to find any significant relationship [18]. In a third paper Koelle *et al.* (2005) [20] model very long time periods, more than a year, in Bangladesh. This model also uses seasonal precipitation and models changes in the susceptible fraction of the population due to demographics and loss of immunity.

1.2. The Model

In this paper, we use detailed and current rainfall, temperature, and predicted tides to model cholera in the Artibonite and Ouest regions. This paper is the first, that we know of, that uses tidal range in a model of cholera dynamics. We forego a bacterial or contaminated water compartment in favor of a saturating infectious compartment with a time delay. This has the advantage of more tractable temporal estimates without over parameterizing and including compartments that are essentially unmeasurable.

These long-term trends and environmental influences establish the pattern of response of the epidemic in Artibonite and Ouest. Thus, parameters were chosen and model calibration set prior to a vaccination program being implemented. We then used the model to evaluate the performance of the vaccination program against the backdrop of an alternative history without vaccination.

2. Material and Methods

For Ouest and Artibonite, we investigated the correlations between reported cholera cases and rainfall, temperature and, in the case of Ouest, tidal range. We wanted to determine.

- if such correlations exist,
- the time delay between environmental conditions and recorded cholera outbreaks, and
- if the effectiveness of a recent vaccination program could be assessed by use of this model.

2.1. Model

Our modeling approach is a modification of SIR type models, where individuals move from susceptible (S) to infected to recovered (R) classes. Conceptually, the underlying model is a variation on the SIWR model, which assumes that cholera is spread through susceptibles' contact with contaminated water, food or fomites. SIWR models use the amount of water consumed as a proxy for all possible modes of transmission, and the concentration of bacteria in the water consumed modifies the infection rate by a dose-response expression (see [8] with a base model [7]). An infectious individual may either be symptomatic (I) or asymptomatic (A) [21]. The probability, ρ, of asymptomatic infection is 0.79 [21,22]. Both symptomatic and asymptomatic individuals move to the recovered group, R, at a rate γ. Symptomatic individuals die from cholera at a rate μ. Transmission rates, $\beta(t)$, are estimated by fitting the number of cases predicted by the model (both incidence and cumulative cases) to the data. A schematic of the system is given in Figure 1.

We chose not to incorporate water bodies and environmental bacterial populations explicitly, since this requires the estimation of extra compartments and a half dozen or so other parameters for which there are no data. The overall impact of having water bodies and bacteria concentrations is that there is a saturating effect on the force of infection, since the probability of getting an infectious dose from contact

with a given body of water (or other sources) necessarily asymptotes as the concentration of bacteria increases (as an absolute limit, it cannot exceed one). Thus, it seems reasonable to replace water bodies and bacteria with a saturating function (J) of the time delayed number of infected people; this has the advantage of eliminating superfluous variables and parameters, while retaining the essential dynamics. Time lags are also included in the action of precipitation and tides. These and all other parameters are discussed below, and values are given in Tables 1 and 2.

Table 1. Parameter values obtained from the literature, simple calculation or by definition (sources are in the last column).

Parameter	Artibonite	Ouest	Units or Calculation	References
ρ	0.79	0.79	fraction becoming asymptomatic	[21,31]
γ	1.4	1.4	fraction recovered per week	[7,9,10]
φ	0.01	0.01	fraction losing immunity per week	[32,33]
N_0	$1,571,020$	$3,664,620$	–	[4]
Λ	0.00045	0.00045	fraction births per week	[34]
μ_0	0.00015	0.00015	fraction deaths (non-cholera) per week	[34]
S_0	$1,534,338$	$3,663,699$	$N-(A_0+I_0+R_0+D_0)$	
I_0	7653	193	regression on early hospitalized cases	[6]
A_0	$28,790$	726	$\frac{\rho}{1-\rho}I_0$	
R_0	0	0	–	
D_0	239	2	–	[6]
t_0	17 October 2010	17 October 2010	290th day of the year	[6]

Table 2. . Numbers in parentheses are the 95% confidence intervals (CIs).

Parameter	Artibonite	Ouest	Units	Description
u_0	0.091 (0.02)	0.144 (0.02)	unitless	initial core fraction.
θ_p	4.980 (0.17)	2.290 (0.27)	weeks	averaging window for precipitation
τ_p	3.381 (0.05)	5.140 (0.21)	weeks	delay for precipitation effects
k	0.441 (0.13)	0.373 (0.13)	unitless	temperature-precipitation interaction level
α	$9.544\ (1.45)\times10^{-3}$	$2.200\ (0.62)\times10^{-3}$	week^{-1}	infection rate
θ_m	–	0.984 (0.69)	weeks	averaging window for tidal range
τ_m	–	1.960 (0.47)	weeks	delay for tidal range effects
c	–	0.147 (0.28)	unitless	effect of tide relative to rain
M_0	–	25.74 (13.5)	cm	baseline of tidal range effect
r	0.0562 (0.006)	0.0376 (0.005)	week^{-1}	decrease in non-core per week
K_I	~0	291.69 (117.9)	number	half saturation constant
ν	0.675 (1.03)	0.703 (1.95)	unitless	efficacy of vaccine

Figure 1. A compartmental model describing the movement of individuals from susceptible to infectious to recovered, with two infectious classes, symptomatic and asymptomatic; a transitional main population in which conditions improve over time and an intractable indigent core. Compartment J is the time-delayed effective infectious class that replaces explicit water bodies and bacterial compartments (see text).

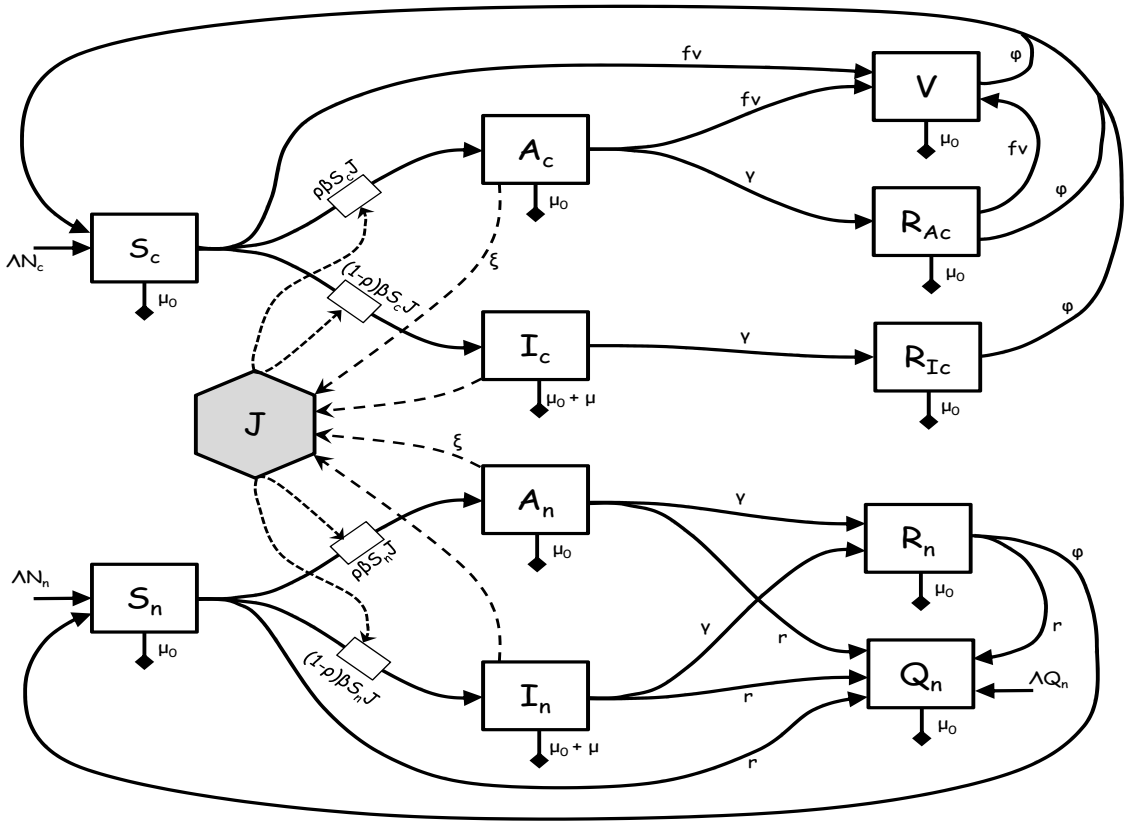

This paper evaluates Artibonite and Ouest separately, in order to capture the different dynamics in each region. In each case, we use the following system of non-autonomous ordinary differential equations and the components to be fitted: t is time since the beginning of the epidemic (week starting 17 October 2010) and Δt is the time interval for reporting new cases (one week).

System of equations.

Core population.

$$\left\{\begin{array}{l}
\frac{dS_c}{dt} = \Lambda N_c - \beta(t)\, S_c J - f\nu(t)\, \frac{S_c}{S_c+A_c+R_{Ac}} - \mu_0 S_c + \varphi\left(R_{Ac} + R_{Ic} + V\right) \\
\frac{dA_c}{dt} = \rho\beta(t)\, S_c J - f\nu(t)\, \frac{A_c}{S_c+A_c+R_{Ac}} - (\gamma + \mu_0)\, A_c \\
\frac{dI_c}{dt} = (1-\rho)\beta(t)\, S_c J - (\gamma + \mu + \mu_0) I_c \\
\frac{dR_{Ac}}{dt} = \gamma A_c - (\varphi + \mu_0)\, R_{Ac} - f\nu(t)\, \frac{R_{Ac}}{S_c+A_c+R_{Ac}} \\
\frac{dR_{Ic}}{dt} = \gamma I_c - (\varphi + \mu_0)\, R_{Ic} \\
\frac{dV}{dt} = f\nu(t) - (\varphi + \mu_0)\, V \\
N_c = S_c + A_c + R_{Ac} + R_{Ic} + V
\end{array}\right\}$$

Non-core population.

$$\left\{\begin{array}{l} \frac{dS_n}{dt} = \Lambda N_n - \beta(t)\, S_n J - r S_n - \mu_0 S_n + \varphi R_n \\ \frac{dA_n}{dt} = \rho\beta(t)\, S_n J - (\gamma + \mu_0 + r)\, A_n \\ \frac{dI_n}{dt} = (1-\rho)\beta(t)\, S_n J - (\gamma + \mu + \mu_0 + r) I_n \\ \frac{dR_n}{dt} = \gamma(A_n + I_n) - (\varphi + \mu_0 + r)\, R_n \\ \frac{dQ_n}{dt} = r(N_n + I_n) + (\Lambda - \mu_0)\, Q_n \\ N_n = S_n + A_n + R_n \end{array}\right\}$$

Infectious population.

$$I(t) = I_c(t) + I_n(t) + \xi\,(A_c(t) + A_n(t))$$

$$J(t) = \frac{I(t-\tau_p-\theta_p)}{K_I + I(t-\tau_p-\theta_p)}$$

Variables to be fitted.

$$\left\{\begin{array}{l} \text{new cases} = (1-\rho)\int_{t-\Delta t}^{t} \beta(\mathfrak{t})\, S(\mathfrak{t})\, J(\mathfrak{t})\, d\mathfrak{t} \\ \text{total cases} = (1-\rho)\int_{0}^{t} \beta(\mathfrak{t})\, S(\mathfrak{t})\, J(\mathfrak{t})\, d\mathfrak{t} \end{array}\right\}$$

2.2. Environmental Effects

Significant rain events will cause overflowing of river and stream banks, which we assume will increase direct contact with the bacteria via contaminated water, or indirectly via soils, vegetation and pathogen-carrying insects, *etc.*, that have been contaminated or have consumed cholera bacteria. We also assume that temperature plays a role by increasing the infection rate. Warmer temperatures result in more rapid growth, better survival and more active bacteria and transmission agents. People also more frequently contact sources of contamination due to the variety of increased activities that warmer weather engenders.

Additionally, in the Ouest region, there are commercial areas, tent-cities and slums that have raw waste directly discharging to Port-au-Prince Bay or to the bay via rivers (e.g., Froide, Momance and Grise), as well as numerous open sewage canals. We hypothesize that there may be additional disease generated when large tidal ranges stir up contaminated sediments or cause blooms of plankton in these coastal or estuarine waters (we tested tidal height and found no association). Again, the chain of infection may be complex and include contact with water, insects, plankton, benthos or consumption of contaminated seafood, *etc*. [19,23,24] Why tidal range would have a significant effect and not tidal height is curious. There are a number of possible explanations. It may be that bottom sediments possibly contain cholera biofilms [25] or copepods hosts. A greater tidal range would scour a larger bottom area by the breaking surface waters along the beaches, or more fresh and brackish water from river outflows and estuaries can contact the bottom sediments as the water falls and rises again, or a combination of actions. In any event, these are just speculations, and the association noted here may warrant closer examination in the field.

To incorporate these effects, we modify the transmission rate, β, as follows:

$$\beta(t) = \alpha \left[H(t)\, P(t - \tau_p, \theta_p) + cM(t - \tau_m, \theta_m) \right] \tag{1}$$

where P is a moving average of the amount of daily rainfall, M is a moving average of the maximum semi-diurnal tidal range, H is a heat index based on mean air temperature, τ_p is the lag time for precipitation, τ_m is the lag time for tides, θ_p, and θ_m are the respective averaging periods, α is a proportionality constants and and c is the strength of the tidal effect relative to precipitation.

The population is split into two sub-populations. The first (core) group includes the worst slums and permanently displaced people living in tent camps or other privations. The other (non-core) group includes all others, from those that may have potentially been at risk only immediately after the earthquake to those that are poor, but have been fortunate enough to, through their own efforts or aid from outside agencies, see continual, albeit incremental, improvements in conditions over time. We include an expression for the improvement of conditions over time by having the number of susceptible or at-risk people reduced directly by public health improvements. This improvement could be due to decreasing the number of people in temporary housing, increased access to clean water, increased personal hygiene, decreased contamination of the environment and rapid treatment of new cases; or any other means of removing risk. We model this by assuming that there is a constant rate of removal of people from the exposed non-core population. We denote r as the rate of improvement in conditions; $1 - u_0$ is the initial fraction of the population whose risk is eradicable, and u_0 is the initial fraction of the population that is chronically indigent. The at-risk population starts out equal to the entire susceptible population and declines asymptotically to the remaining number of indigent susceptibles as conditions improve.

2.3. Data

2.3.1. Cholera Cases

The source of the epidemic data was the Haitian Ministry of Public Health and Population [4] and compiled by the Pan American Health Organization [6]. The available data sets from the above source, used for this study, consist of cumulative cholera cases and new cholera cases. New cholera cases are calculated based on the difference between the latest report and the previous one. The cholera case definition also includes suspected cholera cases and deaths in addition to confirmed cases and deaths. As such, data posted on the website are periodically updated with minor corrections. Cases are reported on a weekly basis, with the reporting week beginning on Sunday.

Reported hospitalized cases and hospitalized deaths are probably more accurate, but for the purposes of this study, less useful, since we want to track the progress of the epidemic, and increases in access to treatment biases the data. No data is available for new or total cases (TC) during the first four weeks; however, hospitalized case data is available. In order to estimate the number of new and total cases during the first four weeks of the epidemic, we calculated the rate of increase of the reported hospitalized cases over the first four weeks and then used these rates to back-calculate the number of cases during the the first four weeks of the epidemic necessary to match the reported numbers for all cases in the fifth week.

2.3.2. Environmental Data

We compared rainfall, temperature and tide data to the pattern of new cholera cases reported each week. The rainfall data comes from NASA [26], using centrally-located points in each region as our datum point, given by (latitude, longitude). For Artibonite, our datum point is $(19.125, -72.625)$ and for Ouest, it is $(18.625, -72.375)$ [26]. Precipitation estimates provided in the TRMM_3B42_daily.007 data product are a combination of remote sensing and ground verified information reported with a spatial resolution of 0.25×0.25 degrees and a temporal resolution of 1 day; further details are available on the website [26].

Temperature data is mean daily air temperature at Port-au-Prince and is reported by the Weather Underground [27]. We used a sine function fit to the annual cycle in simulations. This has the advantage of allowing us to extrapolate temperature patterns for model projections, while at the same time not severely impacting model performance by including more raw data in the simulations. Unfortunately, only temperatures from Port-au-Prince were available. The temperature index derived from Port-au-Prince data were used for both Ouest and Artibonite.

Tide data is for Port-au-Prince Bay (StationId: TEC4709) [28]. These numbers are predictions from NOAA's tide model for this location and are not direct measurements. NOAA's web site allows one to download tide numbers for any date starting from 2010 and extending through 2014. Again, only data from Port-au-Prince is available. The use of model predictions rather than actual measurements may result in underestimation of the effects during extreme events, such as tropical storms.

2.3.3. Data Analysis

The initial modeling was done by comparing data sets in the frequency (Fourier) domain for new cases and rainfall in order to find any suggestions of matching periodicity and/or time-lags. After that code was written in Berkeley Madonna to simulate the dynamical system and study the environmental data in order to match predictions to data (when we discuss the output of our model, we will use the term "prediction" to indicate the numbers generated during the calibration phase of the model and "projection" to indicate the extrapolation of the model's past cases used for the calibration). Rainfall data was available only to the week of 27 January 2013 (Week 119), because of the lag between the timing of rainfall events and what had been processed at the time we accessed it [26].

2.4. Model Calibration

All modeling and calibration was done in Berkeley Madonna. We used values (or averages of ranges) for all demographic variables, initial values and the three model independent parameters for cholera (fraction asymptomatic, recovery rate and loss of immunity rate) as established by previously published research (ρ, γ, φ, Λ, μ_0, N_0, S_0, I_0, A_0, R_0, D_0, and t_0; see Table 1). Since our model contains several fitted parameters (θ_p, τ_p, k, α, θ_m, τ_m, c, M_0, K_I, r and u_0; see Table 2), we needed to supply a plausible range and initial value for each parameter in order to efficiently search the parameter space for a best fit. These ranges and initial values were chosen by visually fitting the new case output of the model to reported new cases. The Berkeley Madonna curve fitting algorithm was then used to minimize the root

mean square difference between model predictions of the number of new cases for the time delays and averaging intervals (τ_p, τ_m, θ_p, θ_m); these were then fixed, and the number of cumulative cases was fit to reported cumulative cases by adjusting the other parameters (k, α, c, M_0, K_I, r and u_0). Parameter sensitivities were output from Berkeley Madonna at one-week intervals. Confidence and prediction intervals were then calculated using the delta method. [29,30] For example, confidence intervals for the parameter estimates were obtained by inverting the self product of the sensitivity matrix and using the result to estimate the covariance matrix of the model parameters [29]. These errors are only errors from the fitting procedure and do not include the propagation of error from the data themselves (which are unknown).

2.5. Parameters from Literature

Table 1 displays parameter values for each region obtained from published or online sources. The initial population distribution among core or non-core sub-populations was obtained by multiplying each compartment by u_0 or $1 - u_0$, respectively.

2.6. Environmental Components of the Force of Infection

2.6.1. Artibonite

Infections follow a key set of weather and climatic variables. Meteorological influences on the infection rate are a product of the precipitation rate and a heat index. Daily precipitation $p(t)$ [26] is averaged over an interval θ_p, so that the running average precipitation rate is:

$$P(t-\tau_p,\theta_p) = \frac{1}{\theta_p}\sum_{j=0}^{\theta_p} p\left(t-\tau_p-j\right)$$

where τ_p is the delay in the precipitation's affect on the infection rate (see below). For the delay, we used a simple sine function to model a mean temperature index throughout the year (temperature data from [27]). The mean air temperature index is given by:

$$T_{air}(t) = \sin\left(\frac{2\pi\left(7t+187\right)}{365.25}\right), \quad \text{where } t \text{ is in weeks from 17 October 2010}$$

In addition, there is a direct influence of temperature on the infection rate. This would be expected, since warmer temperatures mean faster growth rates for bacteria and some of their invertebrate hosts (bacterial dormancy is probably not an issue, since the climate is tropical) [19,23]. We use a heat index, $H(t)$, rather than temperature itself. This heat index is a linear function of the normalized temperature pattern with a mean (intercept) of 1, and the slope, k, is a parameter to be fit. This index is used as a multiplicative factor modifying the infection rate: the mean temperature has no effect on the infection rate; low temperatures decrease the infection rate, and high temperatures increase it. Thus, we have:

$$H(t) = 1 + kT_{air}(t)$$

Therefore, the infection rate is given by:

$$\beta_A(t) = \alpha H(t)\, P(t-\tau_p,\theta_p) \tag{2}$$

The tide term, $\alpha c M(t-\tau_m, \theta_m)$, is not included, since we had no tidal range data for the Artibonite coast, and the tidal range data we had (Port-au-Prince) was not found to explain a significant amount of variance in the number of cases in Artibonite.

2.6.2. Ouest

For the Ouest region, we use the same formulation as in Artibonite; however, we found that tidal range appeared to significantly affect infection rates, as well. The maximum tidal range each day (there are two) $m\,(t)$ [28] is averaged over an interval θ_m, so the tidal range formula is:

$$M(t-\tau_m, \theta_m) = \max\left\{\left(\frac{1}{\theta_m}\sum_{j=0}^{\theta_m} m\,(t-\tau_m-j)\right) - M_0, 0\right\}$$

where τ_m is the delay in the tide's affect on the infection rate and M_0 is the threshold for tidal range influence. Here, the effect of water temperature on the response in infection rate was not found to be sufficient to warrant adding another function and additional parameters. Thus, the overall infection rate for Ouest is:

$$\beta_O\,(t) = \alpha\,[H(t)\,P(t-\tau_p, \theta_p) + cM(t-\tau_m, \theta_m)] \tag{3}$$

3. Results

3.1. Parameter Fitting and Model Selection

Table 2 displays parameter values for each region obtained through curve-fitting to cumulative reported cases.

Plausible ranges for time lags were initially obtained from the Fourier analysis; then, parameter ranges and initial values were further refined by visually fitting the new cases predicted by the model to the new case data. We then used the Berkeley Madonna curve-fitting routine to find the remaining parameter set that minimized the sum of the square differences (SSD) between model output for cumulative cases and cumulative case data.

The half saturation constant (K_I) for the saturating infected function was very small compared to the numbers of infected people in Ouest and essentially zero in Artibonite (Table 2). This indicates a very weak link between the numbers of infected and transmission rates. It may be that it requires only a handful of new cases to refresh the bacteria in the environment and/or there is a reservoir of viable bacteria in the environment itself (e.g., in plankton). In any event, we can force the dynamics of cholera in these two departments almost entirely by environmental conditions.

The Artibonite model with tide was not included in Table 2, since inclusion of tide only slightly improved the model fit with cumulative cases and did not significantly improve the model fit for new cases (see Tables 3 and 4). The statistics for the model fit are given in the following two tables. Table 3 is for cumulative cases predicted by the model compared to cumulative case data.

Table 3. Model predictions *versus* data statistics for the cumulative number of cases: root mean squared deviations (RMSD), coefficient of determination (R^2). Degrees of freedom for the statistics are adjusted by the number of parameters fit in the calibration process.

All Cases				
Statistic	**Artibonite (Tide)**	**Artibonite (No Tide)**	**Ouest (Tide)**	**Ouest (No Tide)**
Data points	153	153	153	153
Parameters	11	7	11	7
Adj RMSD	1603.78	1686.48	2825.08	3773.74
Adj R^2	0.996	0.995	0.998	0.997

Table 4. Model predictions *versus* data statistics for new cases: root mean squared deviations (RMSD), coefficient of determination (R^2). Degrees of freedom for the statistics are adjusted by the number of parameters fit in the calibration process.

New Cases				
Statistic	**Artibonite (Tide)**	**Artibonite (No Tide)**	**Ouest (Tide)**	**Ouest (No Tide)**
Data points	153	153	153	153
Parameters	11	7	11	7
Adj RMSD	579.79	587.09	1702.26	1868.38
Adj R^2	0.785	0.789	0.476	0.488

For the full model in either region (model including tides), the parameters θ_m, τ_m, M_0 and c are added and the model is re-optimized. For Artibonite, an F-test for the nested models with cumulative cases gives the following results $F = 4.86 \;\; d.f. = (4,\ 142)$, and the p-value is 0.001. For the Ouest region, an F-test for the nested models gives the following results $F = 29.63 \;\; d.f. = (4,\ 142)$, and the p-value is 6.46×10^{-18}, indicating that the tidal data significantly improved the model fit.

Table 4 is for new cases predicted by the model compared to new case data. The F-test for the Artibonite nested models using new cases gives the following results $F = 1.93 \;\; d.f. = (4,\ 142)$, and the p-value is 0.109. For Ouest, the difference is again significant with $F = 8.47 \;\; d.f. = (4,\ 142)$, and the p-value is 3.698×10^{-6}.

3.2. Lag Times

The total delays in response to precipitation and tides are the sum of the averaging window and the delay function. For precipitation in Artibonite, the averaging window is five weeks plus a 3.4-week delay for a total delay range of 3.4 to 8.4, and in Ouest, they are 2.3 and 5.1 weeks, respectively, for a total delay range of 5.1 to 7.4 weeks. Thus, the delays are similar in the two regions. These long delays are similar in magnitude to delays reported from a study of cholera in Zanzibar, East Africa (eight-week delay) [18], but slightly longer than those reported in Bangladesh (four weeks) [19] and much longer

than reported in another study of the Haiti cholera epidemic (four to seven days) [15]. For Ouest, the estimated averaging window and delay from response to changes in tidal range were about one week and two weeks, respectively, or a delay range of one to three weeks total. However, since the influence of tidal range has not been quantitatively reported elsewhere in the literature, we have nothing with which to compare this number.

At the time of this analysis, rainfall data were available only to the week of 29 September 2013 (Week 154, with the lag periods reported above, this brings the simulation out to 27 November for Artibonite and 20 November for Ouest. This is just before the data for new cases ends on 8 December 2013.

3.3. Vaccination

A program to vaccinate the most at risk populations began in the second week of April and ended in mid-June, 2012. Each site (Ouest and Artibonite Departments) vaccinated about 50,000 persons, and each site had about a 91% second dose coverage. The administration of the first dose was staggered by age group (beginning first with 10-year-olds and up), because the Ministry of Health had a measles, rubella and polio vaccine catch-up campaign for children under 10 years of age that was taking place at the same time last April 2012 (communicated by Jordan Tappero, MD, MPH (CDC/CGH/DGDDER, Atlanta, GA, USA), 29 November 2012).

In the Ouest Department, GHESKIO (Groupe Haïtien d'Étude du Sarcome de Kaposi et des Infectieuses Opportunistes) vaccinated adults, adolescents and children over 10 years of age from 12–23 April 2012, and children under 10 from 26 May–3 June. The first dose of vaccine was given to 52,357 persons (of which, 47,520 received the second dose), living in the slums of Port-au-Prince and surrounding villages (communicated by Jean W. Pape, MD (GHESKIO, Weill Cornell Medical College, Port-au-Prince, Haiti), 29 November 2012).

In the Artibonite Department, PIH (Partners in Health) vaccinated 32,183 people in rural Bocozel and 13,185 people in Grand Saline, with 90.8% of those people confirmed to get the second dose (or 41,194 for both locations). The campaign started 15 April 2012, and ran until 10 June 2012. Here, too, children under nine years old were vaccinated in the second half of the time period, because of the MMR and Polio vaccination campaign (communicated by Louise Ivers, MD (Partners in Health/ZL, Cange, Haiti), 29 November 2012).

With these basic facts, we constructed a crude vaccination schedule (Table 5) using the following assumptions:

(1) approximately 25% of the population is under 10 years old;

(2) the second dose was administered 14 days after the first dose was given [35];

(3) the immune response took hold about 8.5 days after the second dose was given [35];

(4) we used the average number of people vaccinated per day over a 12-day period for adults and 9 days for children.

Table 5. Simulated vaccination schedule for Artibonite and Ouest.

Ouest		
Adult $1st$ dose	$39,268$	10 April–23 April
Adult $2st$ dose	$35,640$	26 April–7 May
Adult immune response	65%–85%	4 May–15 May
Child $1st$ dose	$13,089$	26 May–3 June
Child $2st$ dose	$11,880$	9 June–17 June
Child immune response	65%–85%	17 June–25 June
Artibonite		
Adult $1st$ dose	$34,026$	15 April–26 April
Adult $2st$ dose	$30,896$	29 April–10 May
Adult immune response	65%–85%	7 May–18 May
Child $1st$ dose	$11,342$	19 May–27 May
Child $2st$ dose	$10,298$	2 June–10 June
Child immune response	65%–85%	10 June–18 June

We ran simulations following the above schedule as closely as the simulation would allow by subtracting the numbers of at-risk persons (given below) from the susceptible compartment (S).

In Ouest, the vaccination algorithm involved removing 2970 at-risk persons per day starting on 4 May 2012, and ending on 15 May 2012, or 35,640 total (these correspond to the vaccination of persons over age 10). Then, the algorithm removed 1320 at-risk persons per day starting on 17 June 2012, and ending on 25 June 2012, or 11,880 total (children).

In Artibonite, the vaccination algorithm removed 2574.67 at-risk persons per day starting on 7 May 2012, and ending on 18 May 2012, or 30,896 total (over age 10); then, the algorithm removed 1144.22 persons per day starting on 10 June 2012, and ending on 18 June 2012, or 10,298 total (these correspond to the vaccination of the at-risk children). These simulations roughly follow the actual vaccination schedules given in Table 5.

The efficacy of the vaccine (oral Shanchol) is reported to be between 65% and 85% [35]. We fit efficacy as a parameter and found for Artibonite an efficacy of 67.5% and for Ouest 70.3%.

3.4. Simulations and Projections

We list the time line for particular events in Table 6. Curve fitting (parameter estimation) was done between model output and data from Week 3 to Week 155. We refer to model output during the calibration period as "predictions"; simulations from Week 156 through Week 216 are referred to as "projections". We used rainfall data that ended in Week 154 for the delay period. Data for new infections extended to Week 164. By "immune response for first..." and "immune response for last...", we mean that this is when we begin and end removing susceptibles from the at-risk group, respectively.

Table 6. Time line for modeling events.

Event	Date (Week of Epidemic)	
	Artibonite	**Ouest**
Begin epidemic	17 October 2010 (0)	
Begin case data	7 November 2010 (3)	
End model fitting	6 October 2012 (155)	
Immune response for first adult vaccinated	7 May 2012 (81.1)	4 May 2012 (80.7)
Immune response for last adult vaccinated	18 May 2012 (82.7)	15 May 2012 (82.3)
Immune response for first child vaccinated	10 June 2012 (86)	17 June 2012 (87)
Immune response for last child vaccinated	18 June 2012 (87.1)	25 June 2012 (88.1)
End precipitation data	29 September 2013 (154)	
End precipitation data with delay	27 November 2013 (162.4)	20 November 2013 (161.4)
Begin random average rain fall data	28 November 2013 (162.5)	21 November 2013 (161.5)
End case data	8 December 2013 (164)	
End simulation	7 December 2014 (216)	

3.4.1. Predictions Compared to Observations for Cumulative and New Cases

The following Figures 2 and 3 show the model predictions compared to observations for the cumulative number of cases in the Artibonite and Ouest regions, respectively. Similarly, Figures 4 and 5 show the model predictions compared to observations for the new number of cases in Artibonite and Ouest regions, respectively. Prediction intervals were calculated only for the cumulative numbers, since the final model fitting was done on these numbers. Confidence intervals are shown for incidence. The match for the trends in new cases match fairly well: the slope of the expected (model) regressed against observed (data) is nearly one in both departments (see Figures 6 and 7), even though there is a substantial amount of unexplained variance. Whether this is due to the crude spatial resolution or other factors remains to be seen.

Prediction intervals (PIs) on the cumulative number of cases were calculated using the delta method adapted for differential equations (see, for example, Ramsay *et al*. [30]). After 29 September 2013, rainfall data from NASA was unavailable; for simulations after that date, we did 13 runs using rainfall patterns from each of the 13 prior years. The mean of those simulations was used, and the variance of the 13 runs, at each time step, was added to the variance from the estimation procedure before computing the PIs. We also included the upper and lower 95% percentiles of the rainfall patterns on projected new cases.

Figure 2. Artibonite. The predicted cumulative number of symptomatic individuals, against total reported cases to 1 April 2012. Projections are from then to the end of February. Projections using the vaccination schedule (red) begin on 7 May 2012, approximately three weeks after beginning the vaccination program in Artibonite. All projections after 11 November 2012, are based on runs using the prior 13 years of precipitation, and PI's include the variance of those data (see the text).

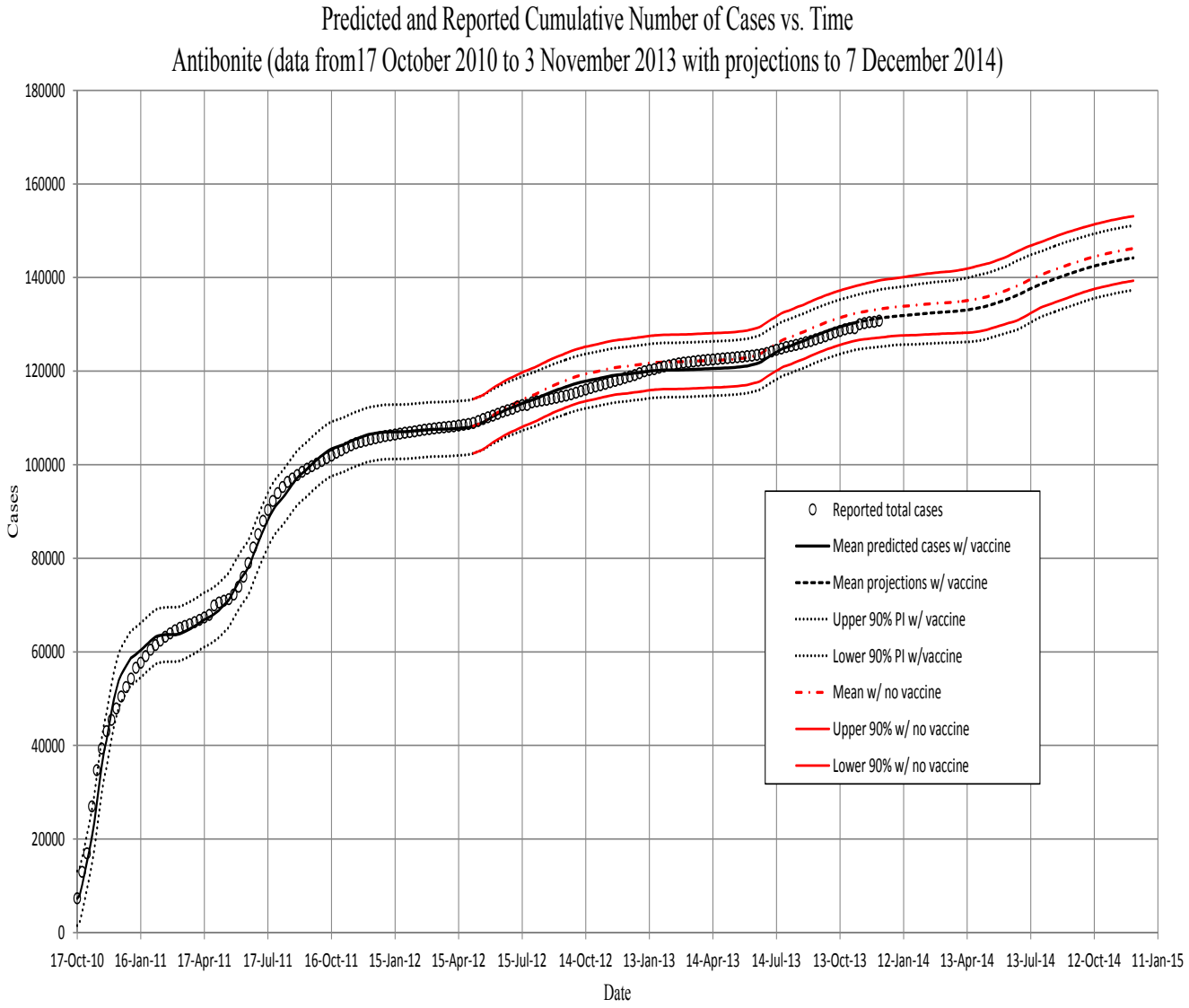

Figure 3. Ouest. The predicted cumulative number of symptomatic individuals, against total reported cases to 1 April 2012. Projections are from then to the end of February. Projections using the vaccination schedule (red) begin on 4 May 2012, approximately three weeks after beginning the vaccination program in Ouest. All projections after 11 November 2012, are based on runs using the prior 13 years of precipitation, and PI's include the variance of those data (see the text). Note that for the Ouest region, the model begins at the fourth week. We assume that the low initial numbers in the first three weeks are a result of the immigration of cases from the Artibonite region. The model therefore uses data for the first four weeks (assumed immigration numbers for the first three weeks and the initialization of the model from data for the fourth week).

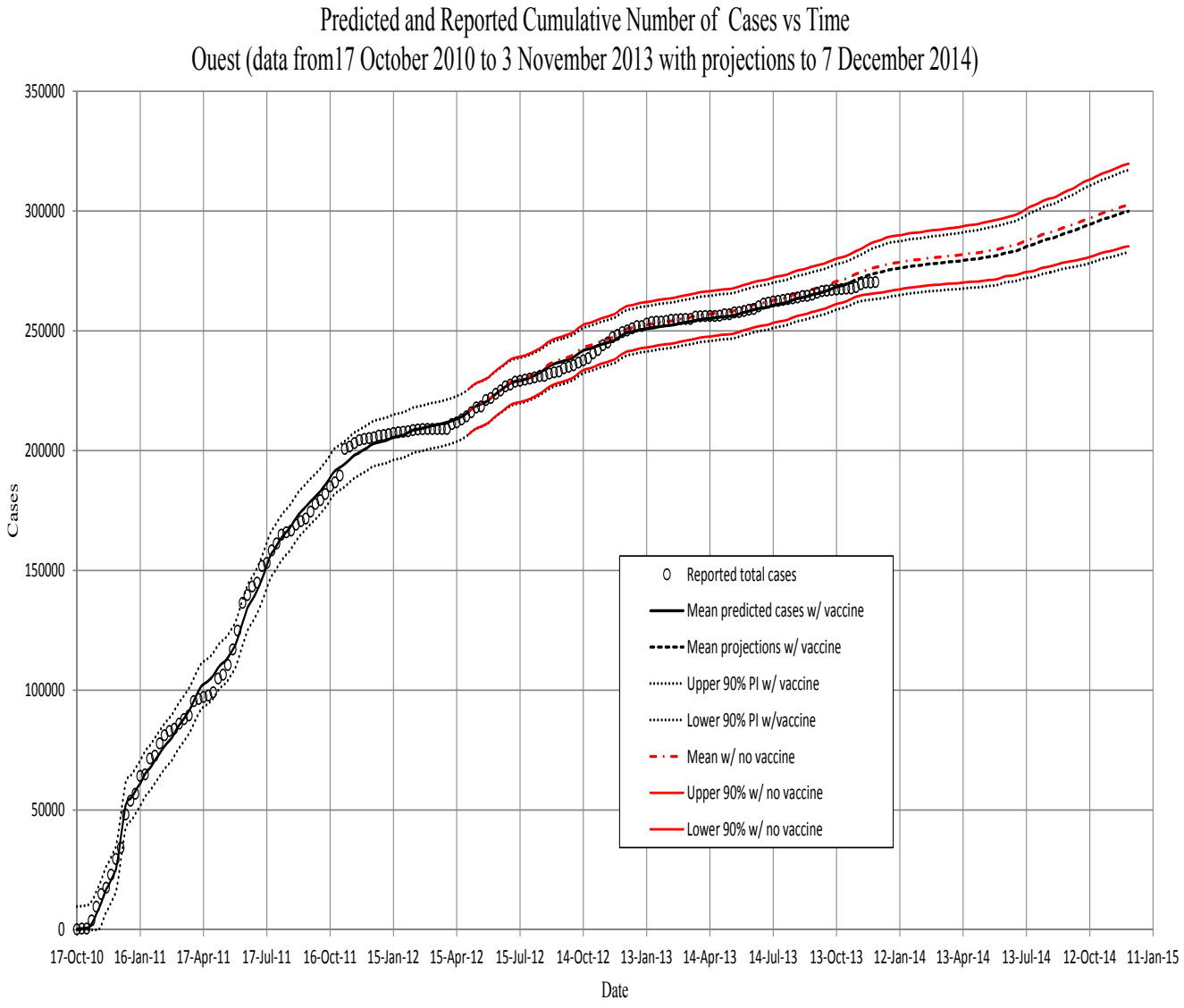

Figure 4. Artibonite. The new symptomatic individuals *vs.* time. Circles, observed; solid line, model prediction; dashed lines, 95th percentile confidence intervals for model projections. The red line is projections with 75 percent vaccine efficacy.

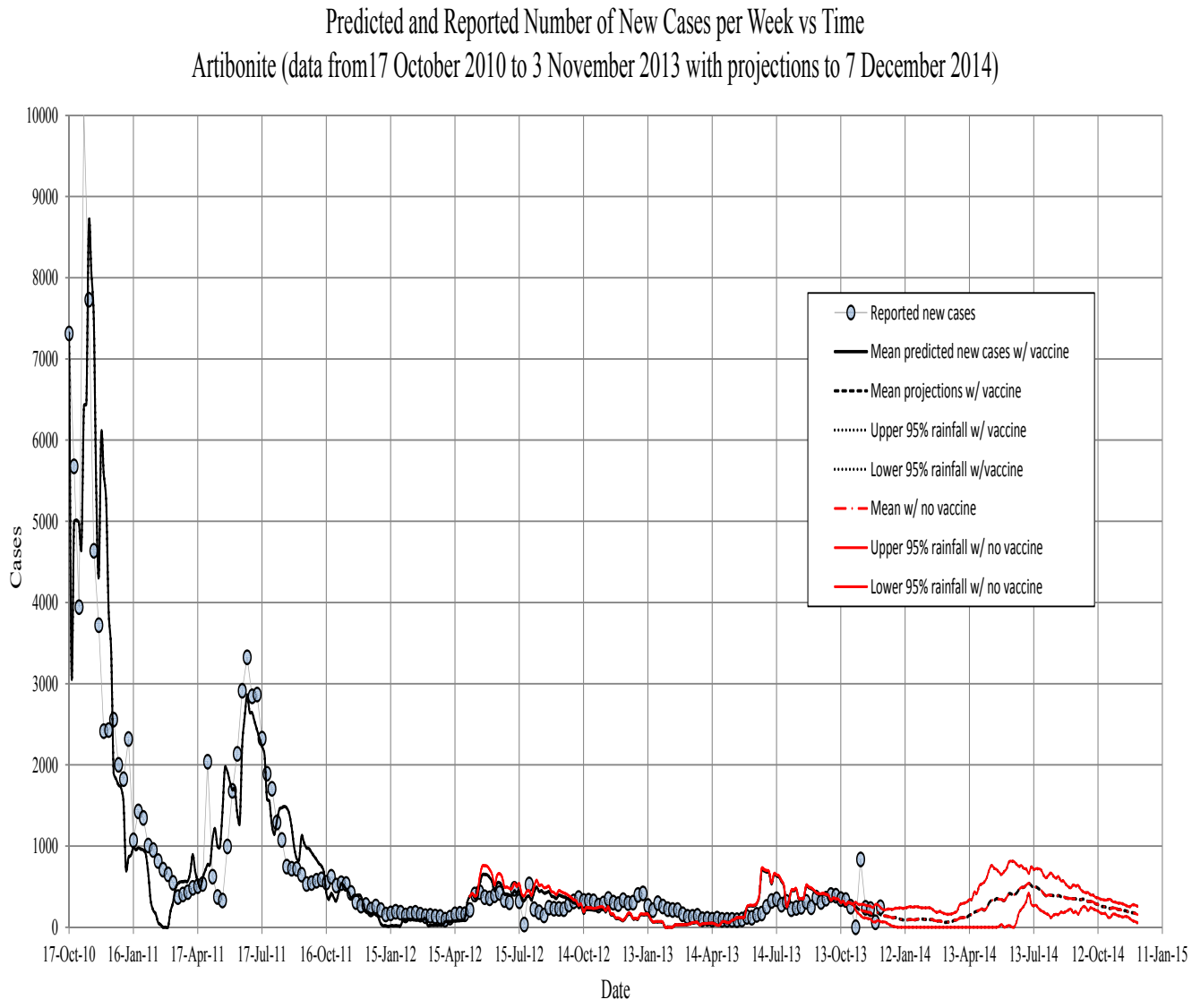

Figure 5. Ouest. The new symptomatic individuals *vs*. time. Circles, observed; solid line, model prediction; dashed lines, fifth, 50the and 95th percentiles for model projections based on the past 13 years of precipitation records.

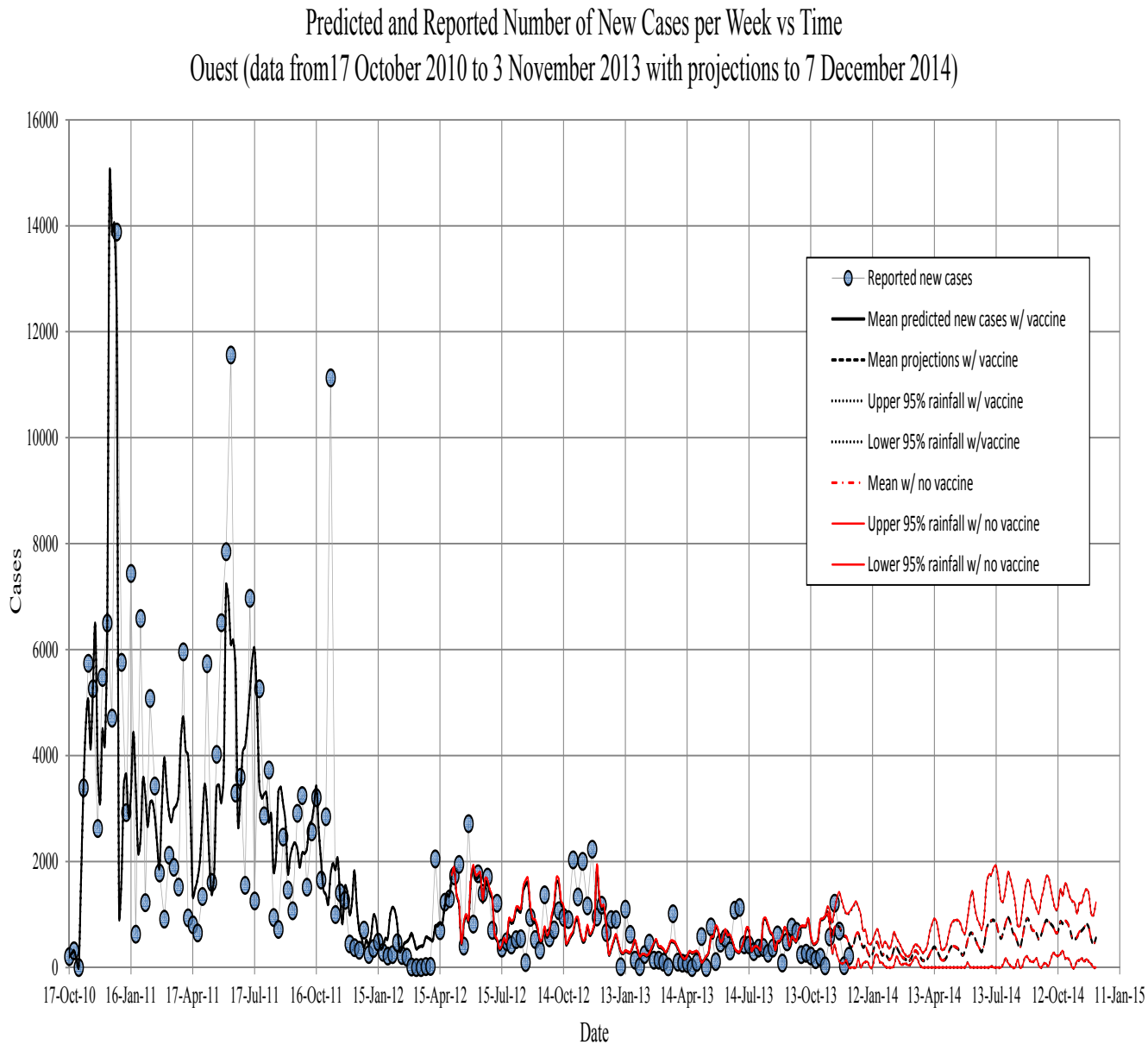

Figure 6. Artibonite. The predicted new symptomatic individuals, against weekly reported cases to 1 April 2012 (square root transformed). A regression line matching the main diagonal $(45°)$ dashed line would show an optimal fit; the discrepancy is due in part to fitting on the cumulative numbers.

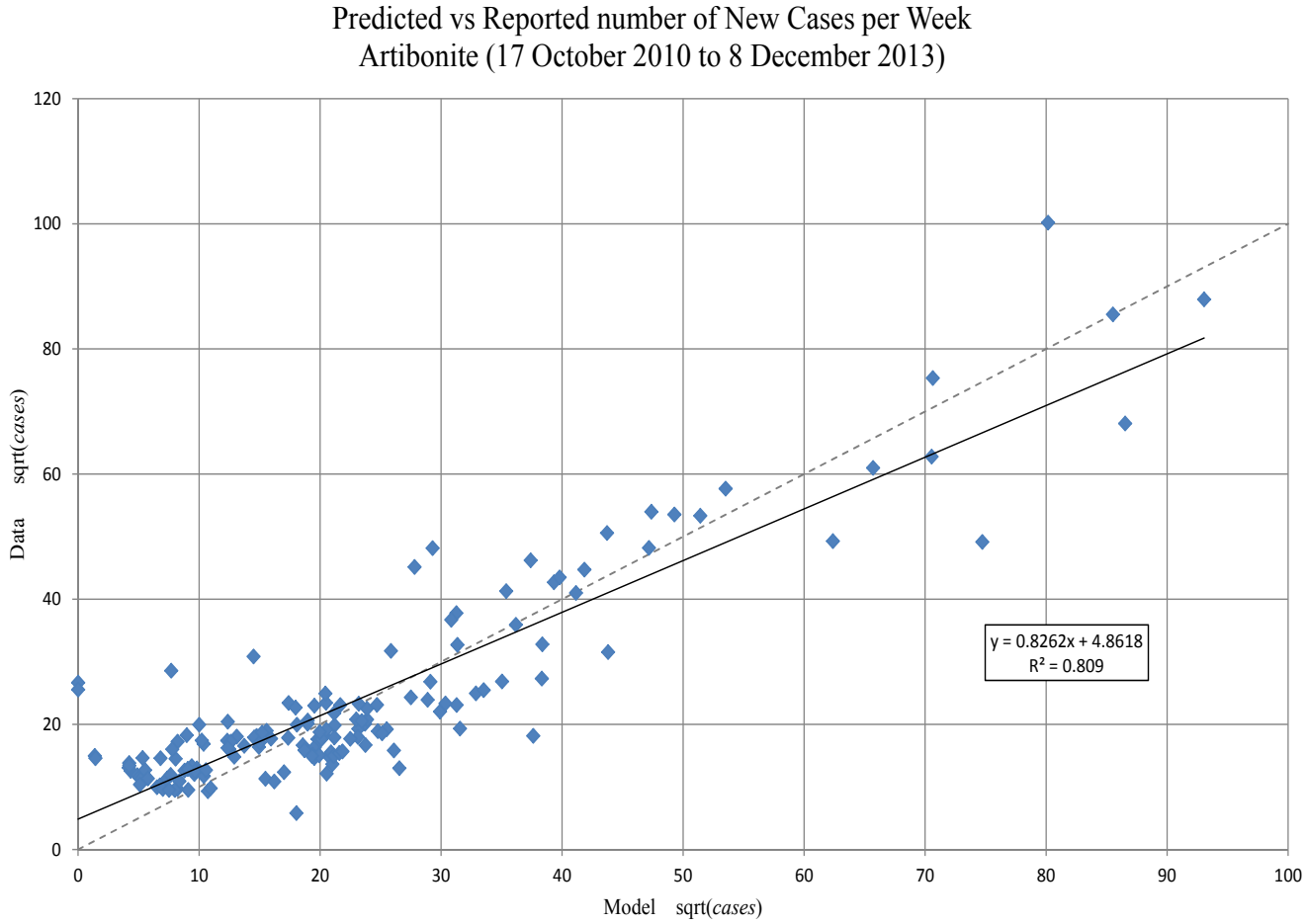

3.4.2. Epidemic Predictions and Projections for Artibonite

The model predicted that by 8 May 2013, one year after the vaccination program, Artibonite would have seen between 117,000 and 128,000 cholera cases without vaccine and between 115,000 and 127,000 with the implemented vaccination program (123,000 thousand actual), a decrease in about 1700 cases (see Figure 8).

According to the model without vaccine, an average of 11,989 people would have gotten sick between 6 May 2012, and 7 November 2012 (six months), and over the same interval with vaccine, an average of 10,375 people would have gotten sick. This represents a 13.5% reduction in the number of people that would have gotten cholera. Between 6 May 2012, and 6 November 2013 (eighteen months), an average of 24,188 people would have gotten sick without vaccine, and over the same interval with vaccine, an average of 22,228 people would have gotten sick. This represents an 8% reduction in the number of people that would have gotten cholera. The maximum percent reduction in the number of cases due to vaccination occurs about 8 August 2012, 13.5 weeks after the assumed beginning of immunity with a 14.5% reduction in cases. Percent

reductions start to taper off after this point, due to the loss of immunity, which is treated as an exponential decay, and the continued occurrence of new cases, which eventually dilutes the effect (see Figure 9).

Figure 7. Ouest. The predicted new symptomatic individuals, against weekly reported cases to 1 April 2012 (square root transformed). A regression line matching the 45° line would show an optimal fit, the discrepancy is due in part to fitting on the cumulative numbers.

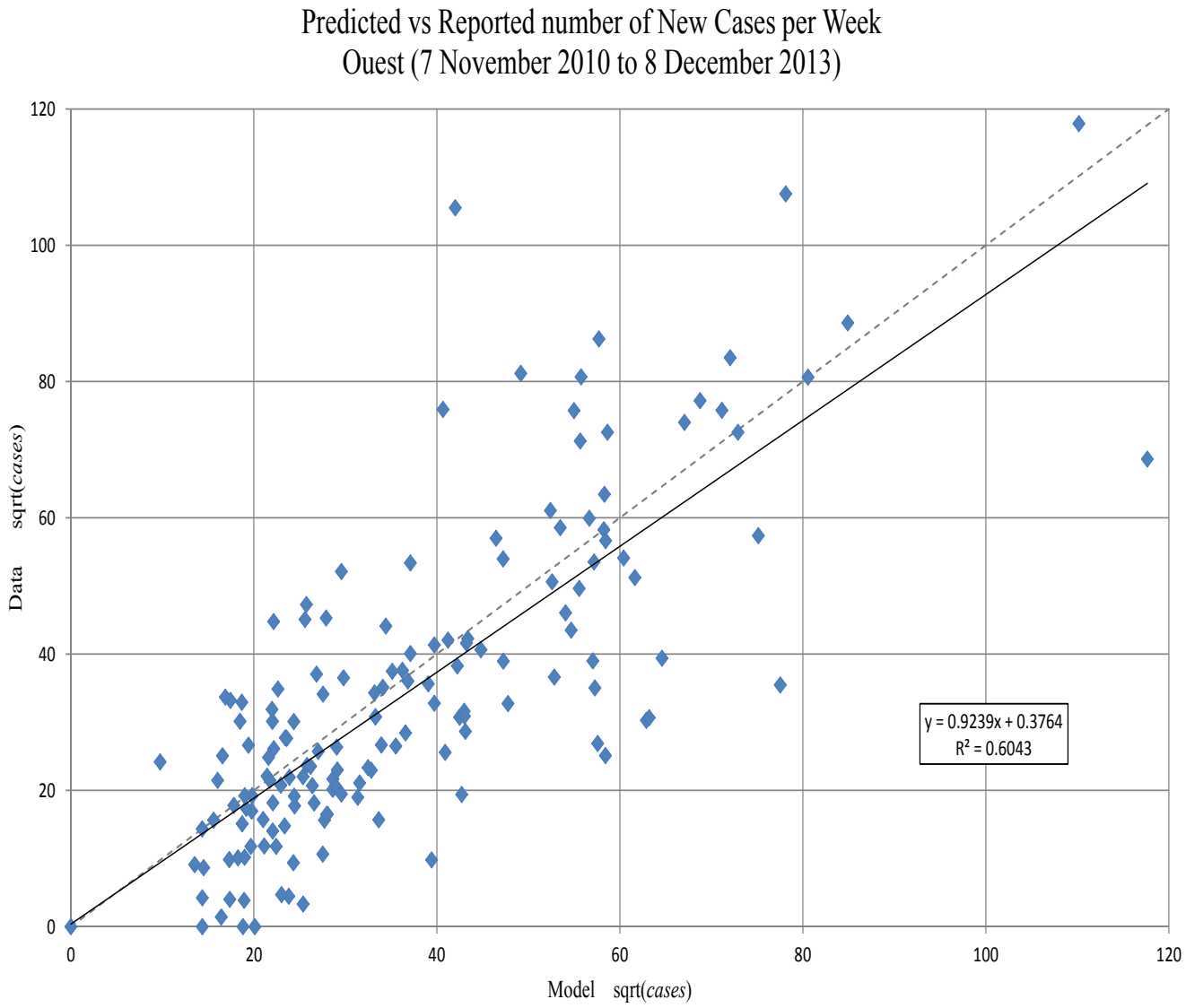

Figure 8. Artibonite. The projected total symptomatic individuals *vs*. time. Circles, observed; solid line, model prediction; dashed lines, fifth, 50th and 95th percentiles for model projections based on the past 13 years of precipitation records. The red lines are the model runs with the vaccination schedule that occurred in spring, 2012 (see the text).

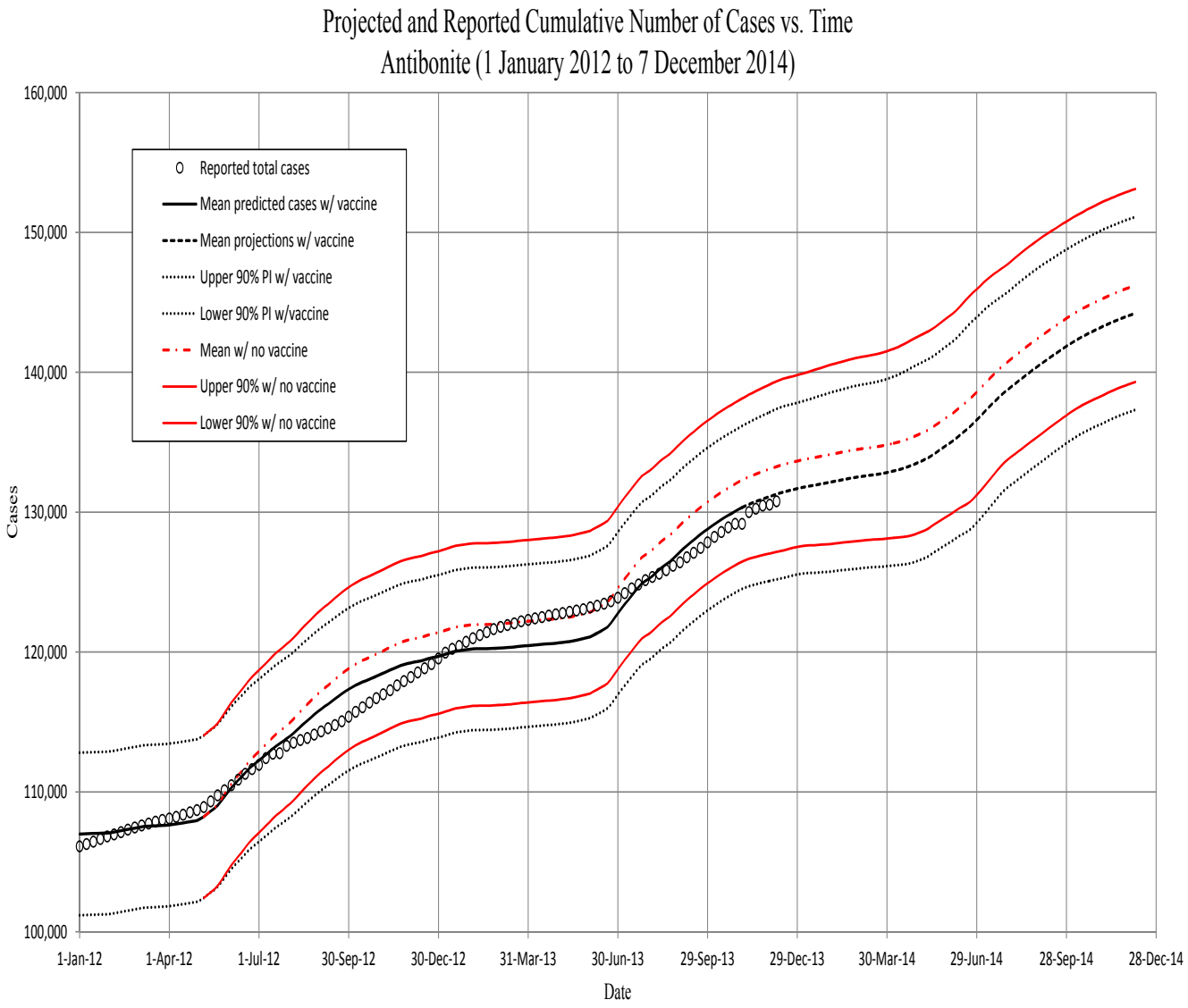

3.4.3. Epidemic Predictions and Projections for Ouest

For Ouest, the model projected that by 5 May 2013, one year after the vaccination program there, Ouest would have seen between 248,000 and 267,000 cholera cases without vaccine and between 246,000 and 265,000 with the implemented vaccination program (257,000 actual), a decrease in about 1900 cases (see Figure 10).

Figure 9. Artibonite. The projected new symptomatic individuals *vs*. time. Circles, observed; solid line, model prediction; dashed lines, 95the percentile confidence intervals for model projections. The red line is projections with 75 percent vaccine efficacy.

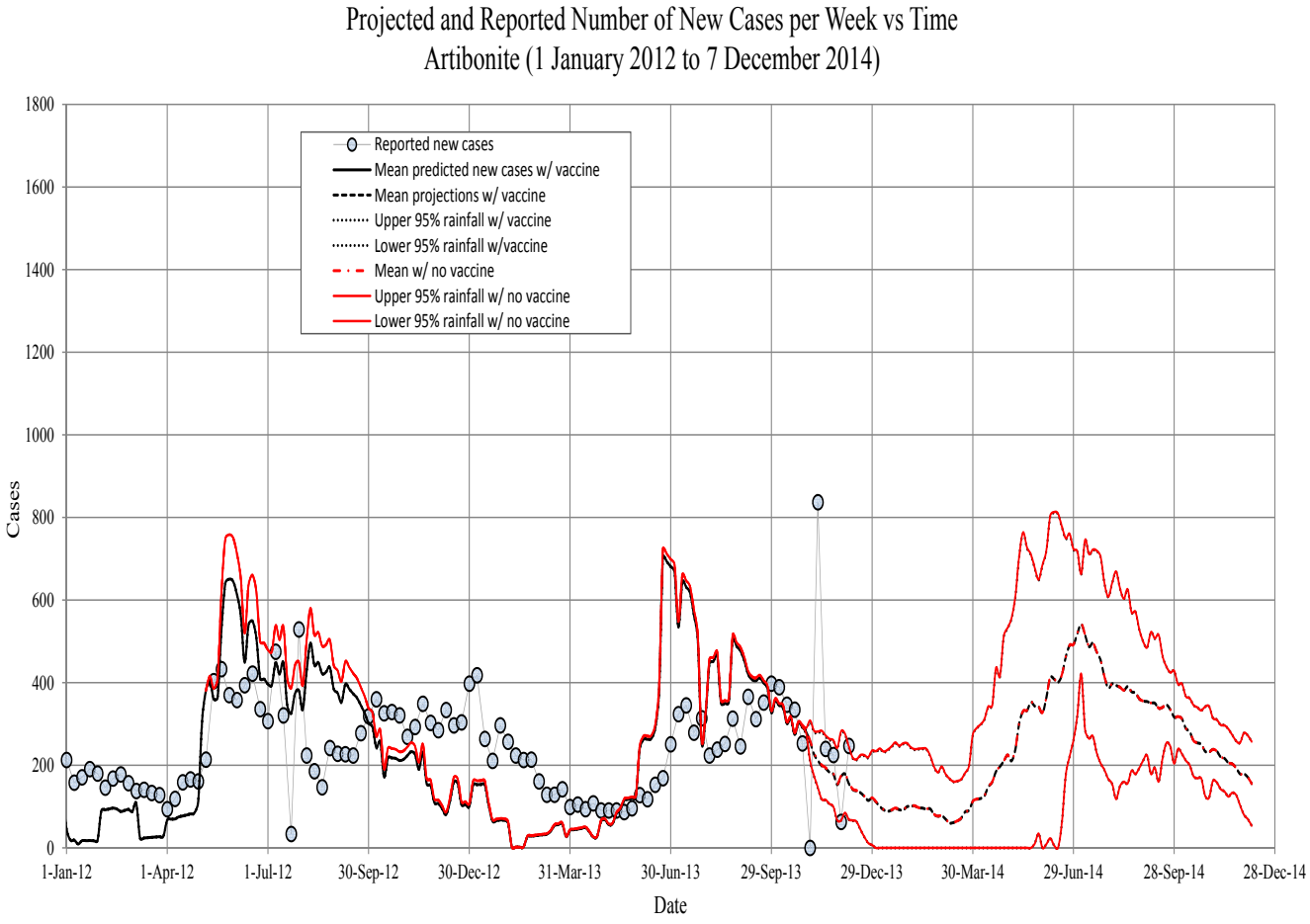

The Ouest model predicts, without vaccine, an average of 28,857 people would have gotten sick between 2 May 2012, and 4 November 2012 (six months), and over the same interval with vaccine, an average of 27,505 people would have gotten sick. This represents a 4.7% reduction in the number of people that would have gotten cholera. Between 2 May 2012, and 3 November 2013 (eighteen months), an average of 56,377 people would have gotten sick without vaccine, and over the same interval with vaccine, an average of 54,003 people would have gotten sick. This represents a 4.2% reduction in the number of people that would have gotten cholera. The maximum percent reduction in the number of cases due to vaccination occurs about 21 November 2012, 29 weeks after the assumed beginning of immunity with a 4.74% reduction in cases. The smaller fraction vaccinated in Ouest also leads to much subtler differences in the incidence. Percent reductions in Ouest start to taper off much later than in Artibonite, since the fraction of the at-risk population protected starts out at a much lower level, and the rate of decay of the effects are subsequently slower (see Figure 11).

Figure 10. Ouest. The projected total symptomatic individuals *vs.* time. Circles, observed; solid line, model prediction; dashed lines, fifth, 50th and 95th percentiles for model projections based on the past 13 years of precipitation records. The red lines are model runs with vaccination schedule that occurred in spring, 2012 (see text). The slow down in growth in late February and March was before the vaccination program began.

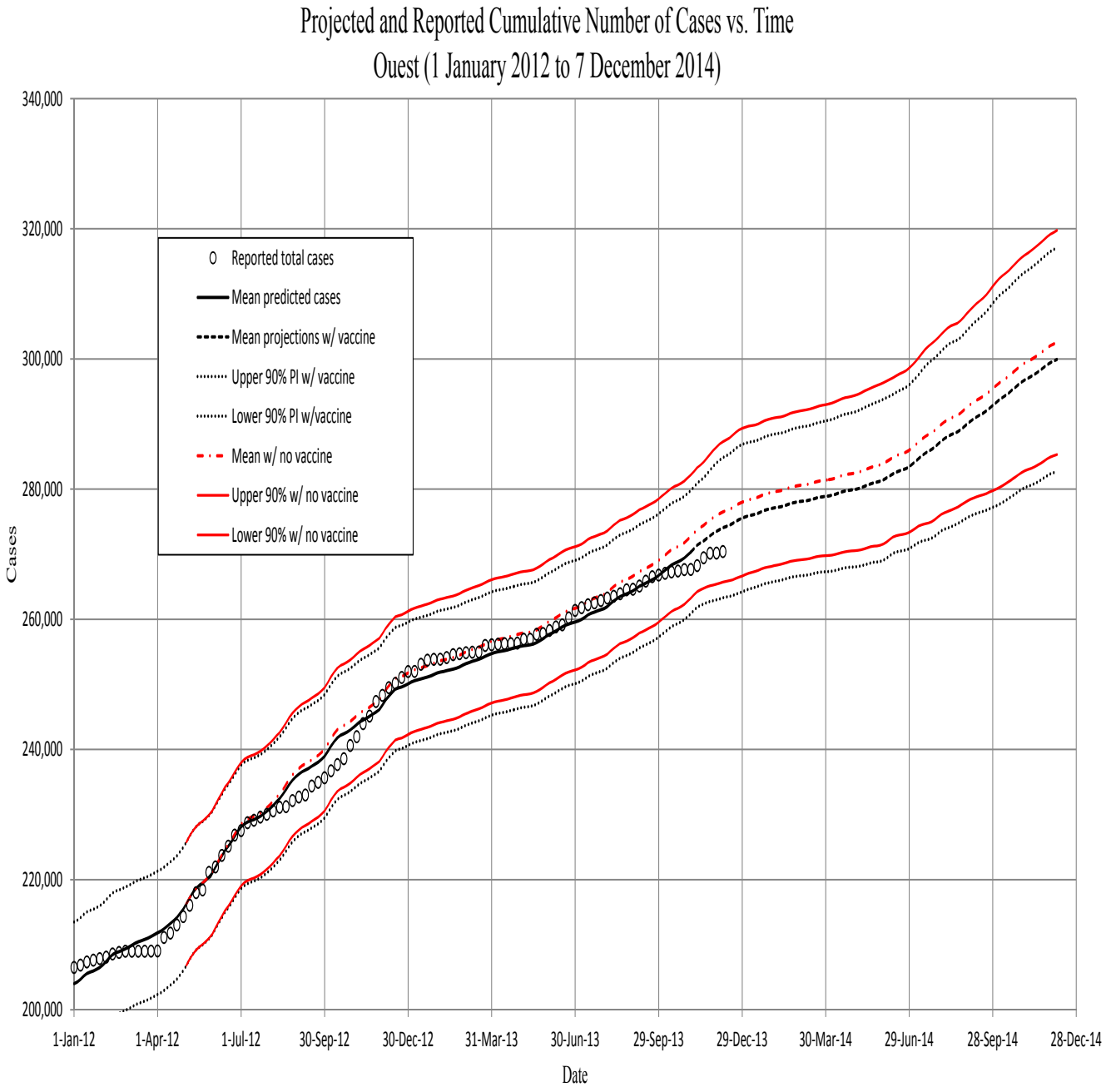

Figure 11. Ouest. The projected new symptomatic individuals *vs.* time. Circles, observed; solid line, model prediction; dashed lines, fifth, 50th and 95th percentiles for model projections based on the past 13 years of precipitation records.

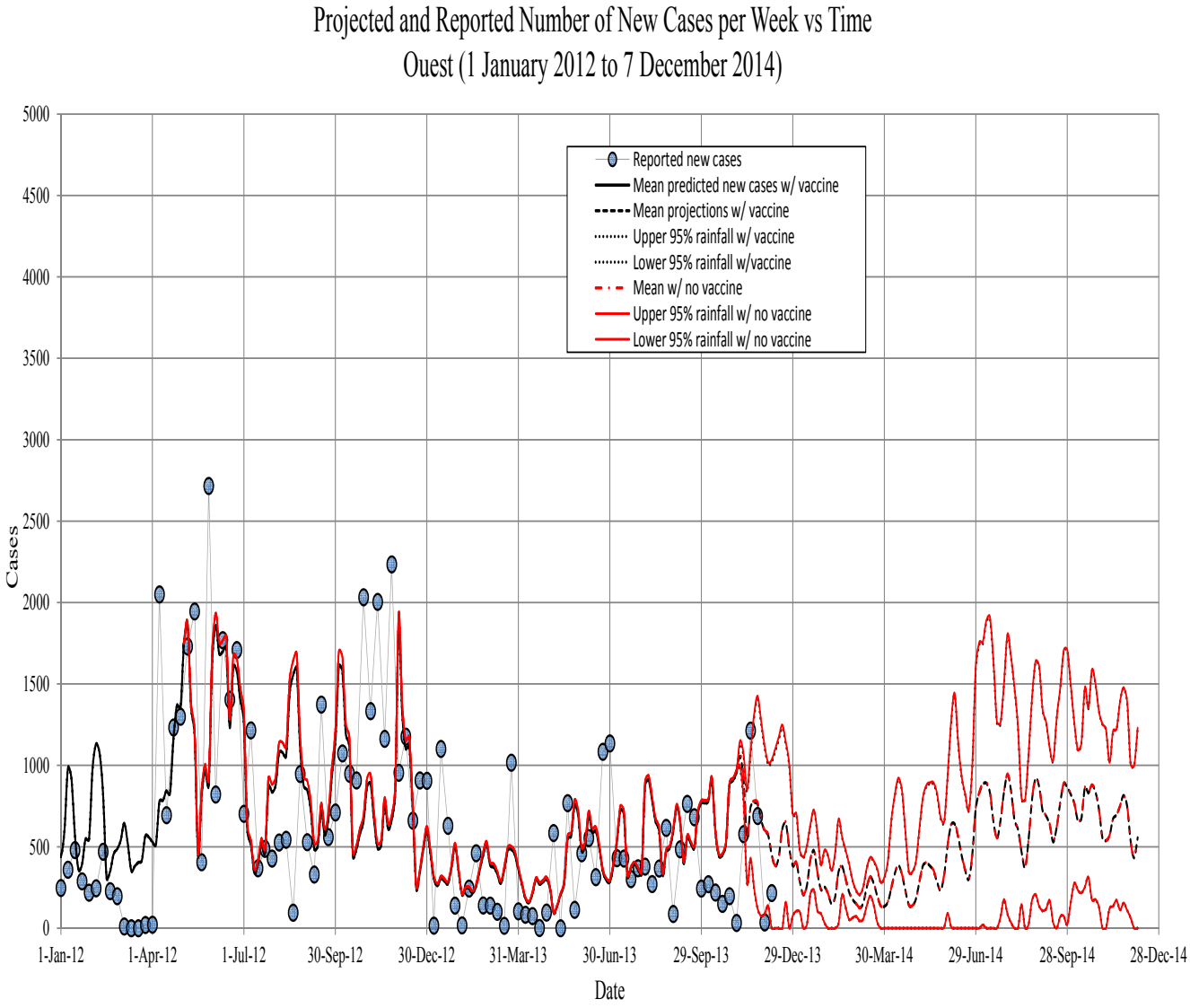

3.5. Vaccination Scenarios

We looked at changing the number of people vaccinated and the timing of vaccination to see if there is some optimal schedule that can be applied.

3.5.1. Changing the Number of People Vaccinated

The first experiment was to change the number of people vaccinated. We completed, in the model, all vaccinations within a five-week period. The second round of vaccination was assumed to begin in epidemiological Week 80, and the immune response was assumed to begin a week later in Week 81, with a 70% efficacy. This was to approximately match the timing of the initiation of the actual vaccination second dose. We varied the numbers vaccinated from 0% to 100% coverage of the non-symptomatic core

group (susceptible, asymptomatic and recovered asymptomatic), in Artibonite and Ouest. The results are illustrated in Figures 12 and 13. Percent coverage of the vaccinated is shown on the x-axis and percent decrease in cases on the y-axis. We show the percent decrease of cases at Weeks 100, 125 and 150 of the epidemic. These correspond to 20, 45 and 70 weeks after beginning administration of the second dose of the vaccine in the $80th$ week.

Figure 12. Artibonite. The percent decrease in the total number of cases at Weeks 100, 125 and 150 for the percent of the non-symptomatic core group vaccinated indicated on the abscissa. The onset of the immune response was assumed to begin in Week 81 and complete in Week 85. We assume 70% efficacy of the vaccine. The actual number completing vaccination (41,194) is indicated by the vertical line.

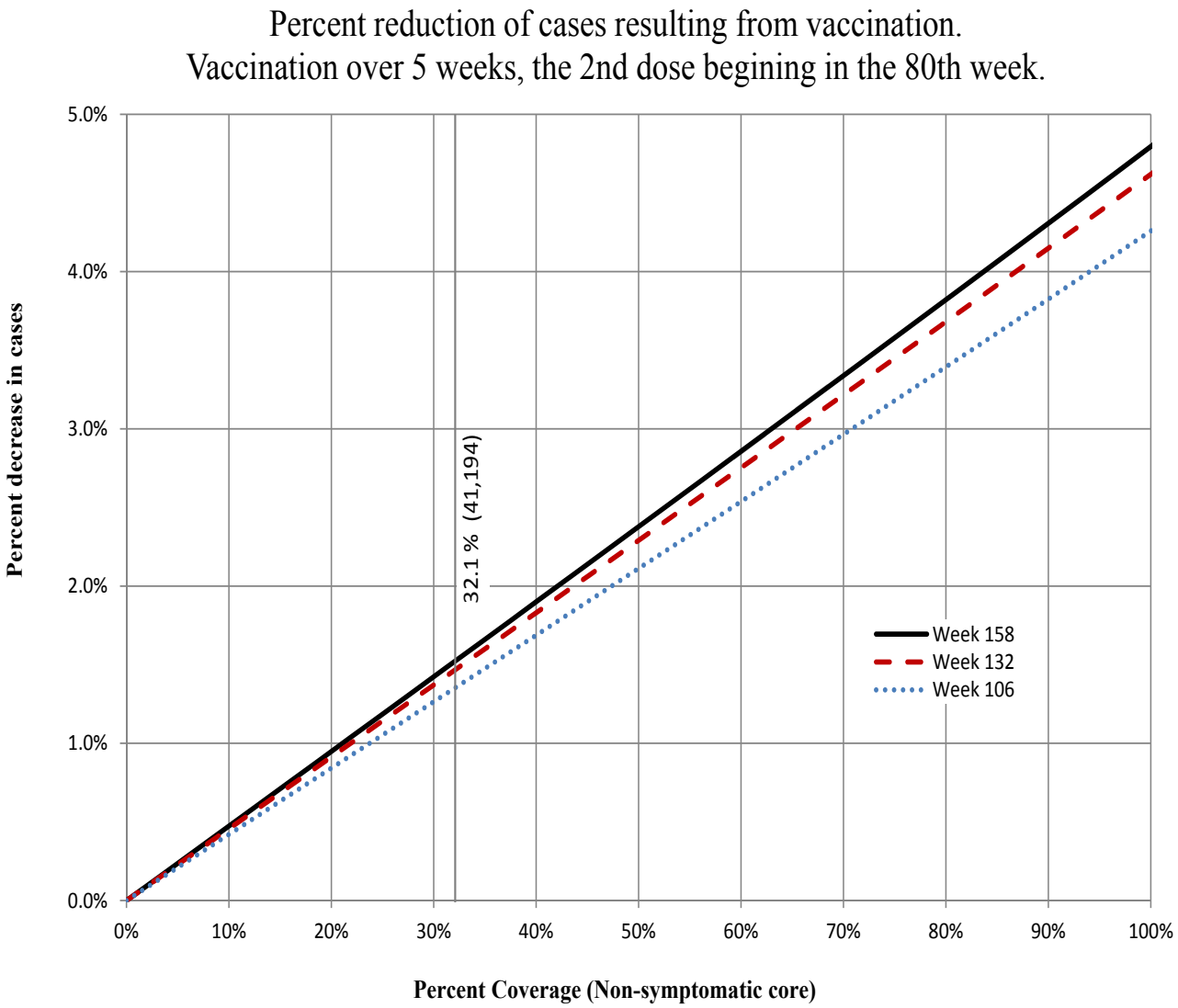

Figure 13. Ouest. The percent decrease in the total number of cases at Weeks 100, 125 and 150 for the percent of the non-symptomatic core group vaccinated indicated on the abscissa. The onset of the immune response was assumed to begin in Week 81 and complete in Week 85. We assume 70% efficacy of the vaccine. The actual number completing vaccination (47,520) is indicated by the vertical line.

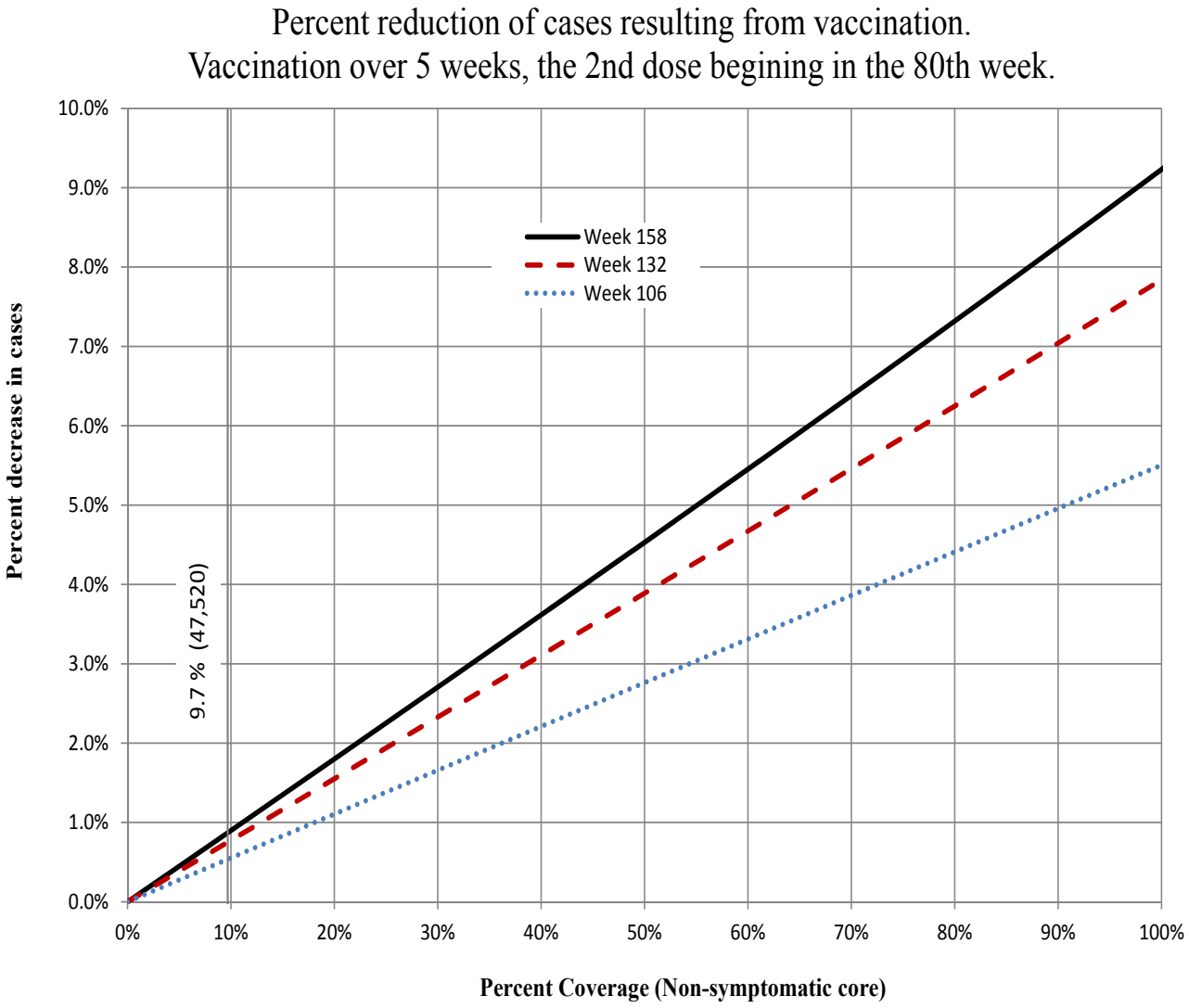

In both departments, the percent decrease in the number of cases increases steadily until the number vaccinated reaches the number of people remaining in the at-risk group. At this point, there are no more people to be vaccinated, but 30% of those people that were susceptible and vaccinated are still susceptible.

The curve increases almost as a straight line (almost, because the vaccination takes place over a finite period of time rather than instantaneously), indicating a constant elasticity of coverage (at 158 weeks, they were 0.048 in Artibonite and 0.092 in Ouest; see Figures 12 and 13 respectively.) and that the potential benefit to each person remains constant (herd effects were minimal). The optimal amount to have vaccinated at 80 weeks would have been three times what was done in Artibonite and ten-fold

greater in Ouest. However, the costs of vaccinating every person at risk (including those that are or were asymptomatic) is certainly not a linear function, and a cost-benefit analysis would be necessary to determine if, and at what point, the money and efforts would be better expended in other control measures.

3.5.2. Changing the Timing of Vaccination

To investigate the best timing of vaccination, we ran two scenarios: the first, vaccination numbers at 100% coverage of non-symptomatic individuals; and the second, vaccination near the numbers actually vaccinated. We graph percent reduction in cases over scenarios without vaccination. In Figures 14 and 15, for example, the curves represent the percent reduction in cases as a function of the week in which the second dose was beginning to be administered. There are four different curves on each graph representing the percent reductions at given intervals ($\frac{1}{2}$, 1, $1\frac{1}{2}$and 2 years) after the second dose of vaccination was begun. We simulated the timing of vaccination so that the beginning of the second round increased in weekly increments from the third week to the 247th week.

Figure 14. Artibonite. The percent decrease in the total number of cases 26, 52, 78 and 104 weeks after the beginning of the second round of vaccination indicated on the abscissa. The onset of the immune response was assumed to begin a week later. We assume 70% efficacy of the vaccine.

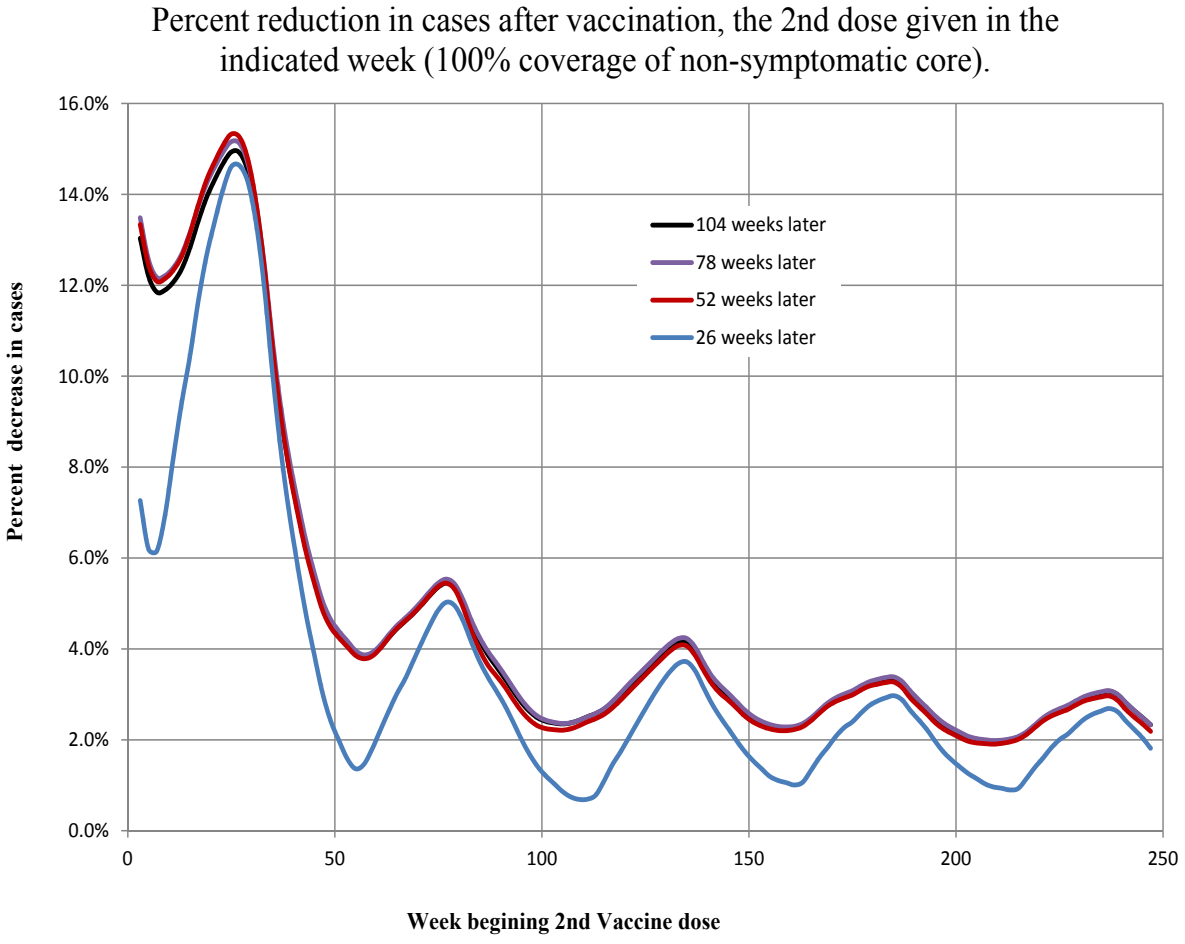

Figure 15. Ouest. The percent decrease in the total number of cases 26, 52, 78 and 104 weeks after the beginning of the second round of vaccination indicated on the abscissa. The onset of the immune response was assumed to begin a week later. We assume 70% efficacy of the vaccine.

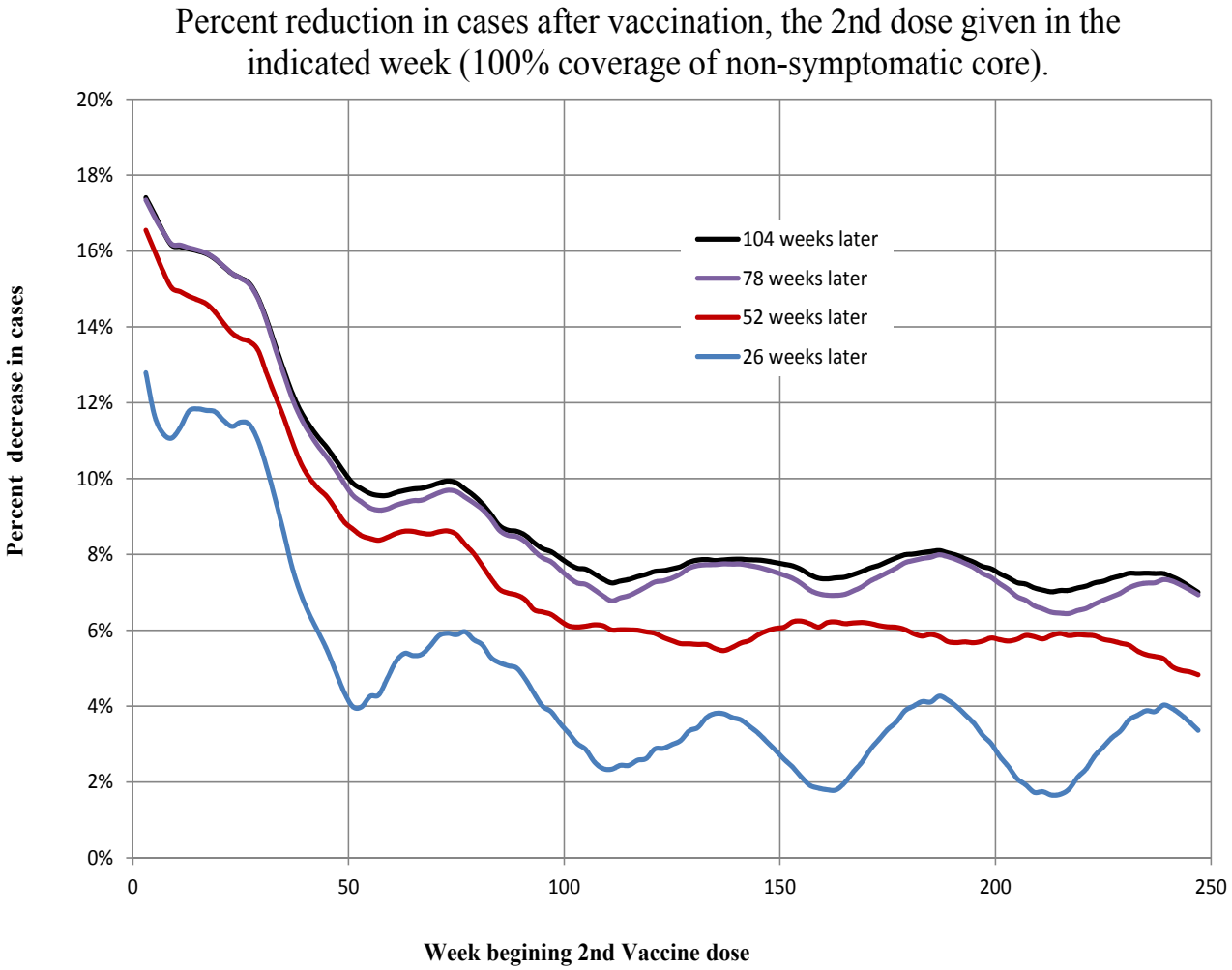

For the first scenario, we simulated the vaccination of the number of non-symptomatic individuals (susceptible, asymptomatic infected and recovered asymptomatic infected) in the core in Artibonite and Ouest. There are two cases for optimizing the timing of vaccination. The first case is to vaccinate as soon as possible after the epidemic begins. Some of the largest percent reductions in the number of cases occur when the vaccine second dose is given between the third and 12th weeks (between 7 November 2010, and 9 January 2011). The second case is to vaccinate in early to mid-spring. Vaccination between the 23rd and 25th weeks (27 March 2011, to 10 April 2011) is both early and seasonal and has the strongest response. As the weeks roll on, the effects of vaccine diminish with subsequent local maxima in occurrence between Weeks 73–77 (11 March 2012, to 8 April 2012), 133–137 (5 May 2013, to 2 June 2013), 185–187 (4 May 2014, to 18 May 2014) and 237–239 (3 May 2015, to 17 May 2015); see Figures 14 and 15. There is a 46% drop between the first spring peak reduction in cases (2011) and the second spring peak reduction in cases (2012) in Artibonite and a 35% reduction in Ouest. After about the 35th

week, percent case reduction subsequently drops about 14% per year in Artibonite and 10% per year in Ouest.

The second scenario (vaccination of 40 thousand in Artibonite and 50 thousand in Ouest) results in similar cases and timing of optimal vaccine administration. See Figures 16 and 17. The amounts of reduction are not only much lower, but the relative effects are reversed. That is, in the first scenario (near optimal numbers), the percent reduction in cases after two years in Artibonite start at 12%–13% when vaccination begins at the outset and decline to 3%–4% when vaccination begins after $4\frac{3}{4}$ years. In Ouest, the percent reduction in cases after two years start at 22%–23% when vaccination begins at the outset and decline to 9%–11% when vaccination begins after $4\frac{3}{4}$ years.

Figure 16. Artibonite. The percent decrease in the total number of cases 26, 52, 78 and 104 weeks after the beginning the second round of vaccination indicated on the abscissa. The onset of the immune response was assumed to begin a week later. We assume 70% efficacy of the vaccine.

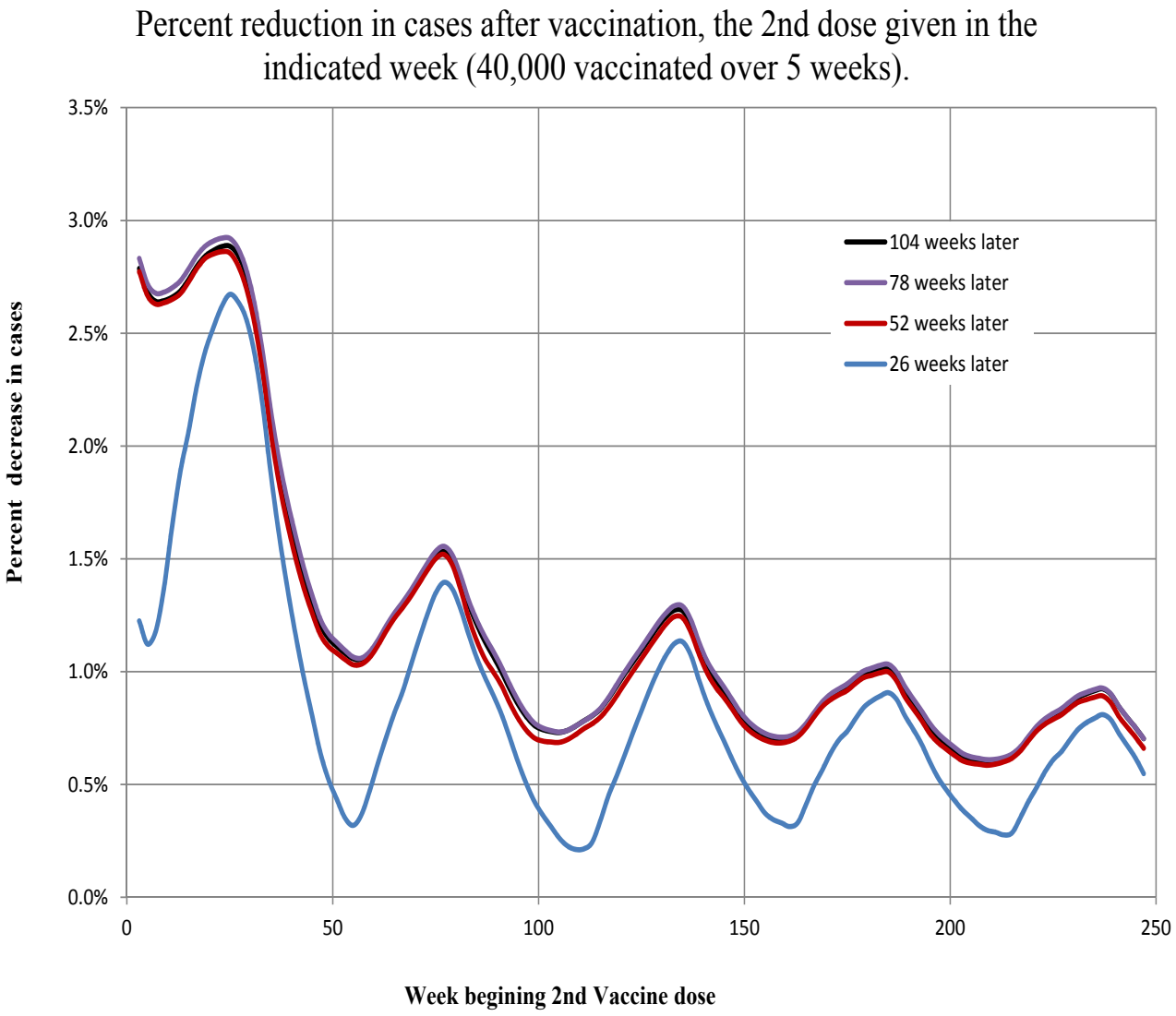

Figure 17. Ouest. The percent decrease in the total number of cases 26, 52, 78 and 104 weeks after the beginning the second round of vaccination indicated on the abscissa. The onset of the immune response was assumed to begin a week later. We assume 70% efficacy of the vaccine.

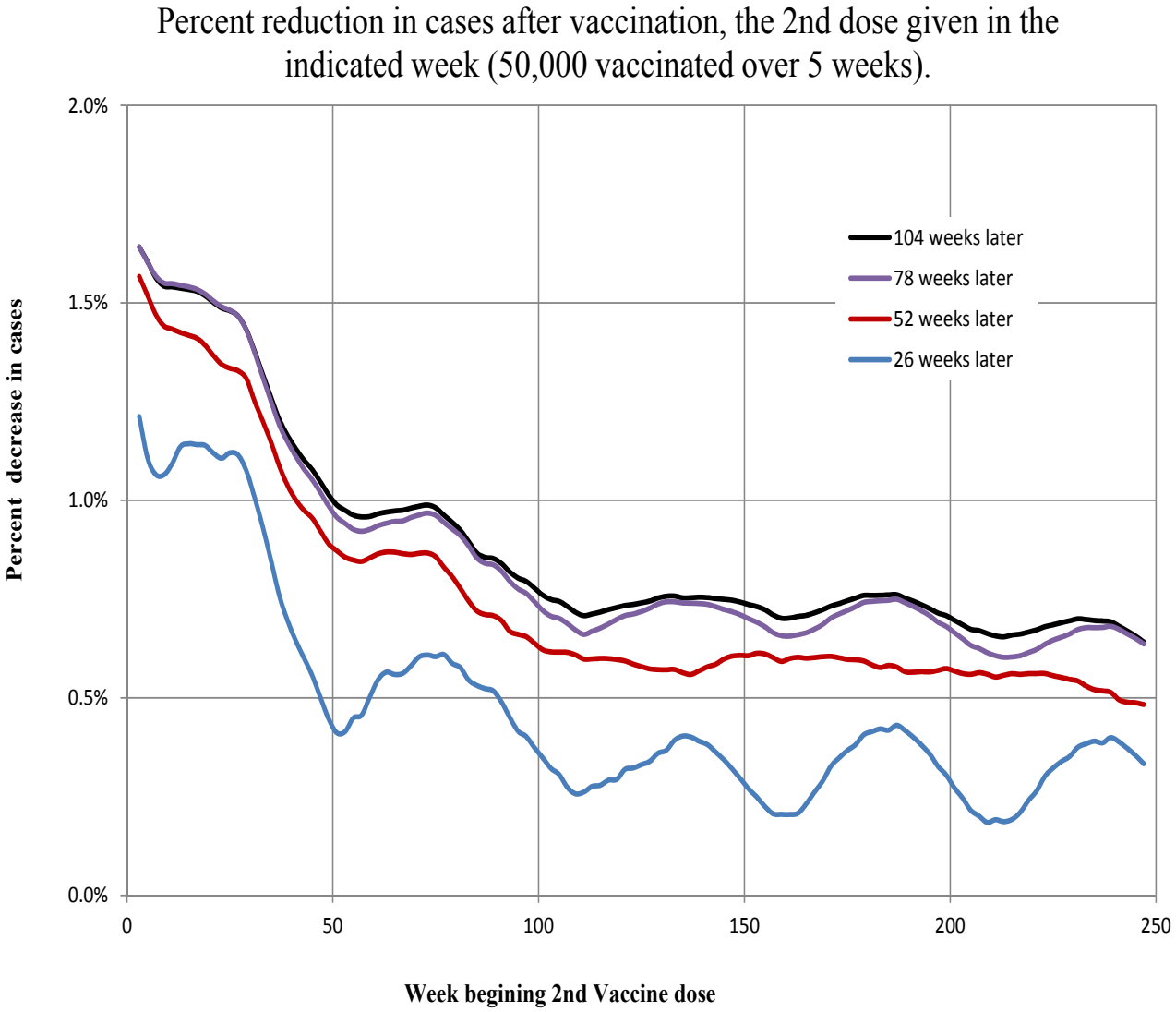

In the second scenario (near actual numbers), the percent reduction in cases after two years in Artibonite starts at 2.6%–2.9% when vaccination begins at the outset and declines to 0.6%–0.9% when vaccination begins after $4\frac{3}{4}$ years. In Ouest, the percent reduction in cases after two years start at 1.6%–1.7% when vaccination begins at the outset and decline to 0.5%–0.7% when vaccination begins after $4\frac{3}{4}$ years.

The actual timing of the vaccination program was approximately Weeks 81 to 83 for adults and 86 to 87 for the second dose. This was about eight to ten weeks past the seasonal optimum, which is not quite halfway between the local crest and trough. Ideally, the vaccination should have been done within a half a year of the start of the epidemic.

4. Discussion

Modeling the dynamics of cholera in Haiti has been hampered by the lack of easily accessible, detailed historical meteorological data. We use NASA satellite data to address this problem. This study shows that with environmental data of sufficient detail and quality, projections of disease progression can be made with sufficient lead time to prepare for outbreaks. The lag times of over five weeks means that if even rudimentary, but reliable, meteorological and coastal records are kept, preparations and resources can be more focused. The gathering of basic weather information is simple and inexpensive and should be made a standard procedure when any agency takes part in interventions, particularly when the environmental component of the epidemiology is so well established.

In addition, we explored the hypothesis that, at least in the Ouest region, tidal influences play a significant role in the dynamics of the disease. It appeared that tidal range rather than the height of the tide itself had the strongest influence. Some connection to tidal influences should be expected where large populations are in close contact with bays and estuaries and humans are consuming local seafood [19,23]. It is not surprising that there was no effect of tidal range found in Artibonite, since the tide model was for off the coast of Port-au-Prince. Again, the lack of readily available detailed historical tide records or even a model for various regions along the coast hinders a thorough investigation of possible factors in the disease dynamics.

Studies from Africa [18] found longer time lags (eight to 10 weeks) and in Bangladesh [19] shorter ones (four weeks). The delays we found in the effects of precipitation on the infection rates were for Artibonite between 3.4 and 8.4 weeks and for Ouest between 5.1 and 7.4 weeks, similar in scale to those studies. However, very short delays (four to seven days) have been reported in a recent study of rainfall forcing in the Haiti cholera epidemic [15]. This study limited the time spans investigated to under 20 days and only during the first year of the epidemic. The authors of that paper also note the discrepancy and suggest that it may reflect the differences between endemic *versus* epidemic situations. An endemic situation would be dominated by rainfall driving transmission through a series of steps, such as washing nutrients leading to plankton blooms, whereas in an epidemic situation, rainfall can bring the population in direct and immediate contact with raw sewage [15]. It would be interesting to investigate whether the delays have become longer as the epidemic has proceeded. It is certainly plausible, since the force of infection was so much higher at the beginning of the epidemic.

Over the course of the epidemic, the incidence has been tapering off. There has been steady and continued effort to improve hygiene and living conditions; however, the areas where the greatest strides are made are those where people leave the camps to return to normal living conditions and employment. The declining numbers of those at-risk in the overall population belie the fact that many local populations are still without basic hygienic facilities. This was reflected in the model by inclusion of the core group, which comprised about 9% of the population in Artibonite and 14% in Ouest. The initial values for these percentages were the u_0 parameters. (The core's percentages varied very little during the course of the simulations. In both departments, the difference between maximum and minimum was only about 0.01%.) These values are somewhat higher than the approximate 5% of the population that OCHA (Office for the Coordination of Humanitarian Affairs - United Nations)reported

in 2012 still displaced from the 2010 earthquake [36]. Of course, the OCHA number is for the entire country of Haiti, not just Ouest and Artibonite.

On top of predicting when and how many cholera cases will increase with Haiti's weather patterns and tides, any modeling to predict the effectiveness of interventions (such as vaccination) should consider these patterns. Considering that cholera may be maintained in the environment outside of the human chain of infection is essential to planing effective prophylaxes and interventions.

Using these models, we were able to do a basic assessment of the relative effectiveness of the recent vaccination program in Artibonite and Ouest. The discrepancy between the apparent effectiveness of vaccination in the two regions is perhaps not that puzzling when one considers the number vaccinated relative to the size of the at-risk population. In Artibonite, about 41,000 people and in Ouest about 47,000 people received both doses of the vaccine. However, our model suggests that in Artibonite, the at-risk population by May 6 was about 65,600, 59,400 of which were in the core population. In Ouest, the at-risk population was still over 379,000 with 295,000 in the core, almost five times the number in Artibonite. In addition, there were approximately 578 asymptomatic core cases in Artibonite and 3439 in Ouest, all of whom would have been eligible to receive the vaccine. Thus, in Artibonite, 69% (40,799) of the most at-risk population apparently received the vaccine, while in Ouest, only 16% (46,974) did. Further, in both regions, 100 people receiving vaccination does not mean 100 people protected. The vaccine was about 68% effective in Artibonite and about 70% effective in Ouest. Therefore, as a rough calculation, we might expect $0.68 \times 40,799 \approx 27,539$ in Artibonite and $0.70 \times 46,974 \approx 32,882$ people in Ouest protected directly.

Yet, of the 40,000 vaccinated in the Artibonite experiments, there is at most 9% (3529/40,000) of those vaccinated not resulting in cases two years hence, leading to a slightly less than 3% reduction in the overall number of cases (Figure 16). This was vaccination at the earliest optimal date. Waiting until the week when actual vaccination occurred, there is about 5% (1919/40,000) of those vaccinated not resulting in cases leading to a 1.4% reduction in the overall number of cases. Thus, for 40,000 vaccinated, 30,000 are protected, and over the following two years, the total number of cases reduced due to this protection is about 2000. In the Ouest experiment, the 50,000 vaccinated there are about 8% (4037/50,000) of those vaccinated not resulting in cases leading to a 1.6% reduction in the overall number of cases (Figure 17). Again, this was vaccination at the earliest optimal date. Waiting until when actual vaccination occurred, there is about 5.2% (2615/50,000) of those vaccinated not resulting in cases leading to about a 1% reduction in the overall number of cases.

5. Conclusions

The complex environmental patterns incorporated in epidemic models allow us to remove a major confounding source of variability and highlight the effectiveness of intervention efforts by identifying deviations from the unaltered flow of events. Contaminated waters persist even when the numbers of infected decline. The resulting dynamics imply that while vaccination can reduce infections and suffering over the span of imparted immunity, without large scale, early, and repeated vaccination, elimination of endemic cholera will only come from substantial improvements in living conditions and public hygiene in impoverished communities.

6. Acknowledgments

The authors would like to thank Scott Braun and George Huffman at NASA, Goddard Space Flight Center, for help accessing precipitation data.

The authors are also grateful to Scott Dowell and Jordan Tappero at CDC, Louise Ivers at PIH and Jean Pape at GHESKIO for information about the cholera vaccination programs in Haiti.

This project was partially supported by a CCFF grant of the Columbian College of Arts and Sciences, of the George Washington University. Svetlana Roudenko was also partially supported by NSF CAREER Grant #1151618 and Stephen Tennenbaum by NSF's Career-life Balance Initiative #1250639.

Author Contributions

Caroline Freitag and Svetlana Roudenko conceived the project and provided the conceptual framework and early modeling efforts. Stephen Tennenbaum and Svetlana Roudenko further developed and refined the model and did the statistical analysis. Stephen Tennenbaum and Caroline Freitag provided background research, data acquisition, and wrote the manuscript with assistance of Svetlana Roudenko.

Conflicts of Interest

The authors declare no conflict of interest.

References

1. World Health Organization. WHO|Haiti. Available online: http://www.who.int/hac/crises/hti/en/ (accessed on 28 April 2012).
2. Cravioto, A.; Lanata, C.F.; Lantagne, D.S.; Nair, G.B. Final Report of the Independent Panel of Experts on the Cholera Outbreak in Haiti. Available online: http://www.un.org/News/dh/infocus/Haiti/UN-cholera-report-final.pdf (accessed on 28 April 2012).
3. Piarroux, R.; Barrais, R.; Faucher, B.; Haus, R.; Piarroux, M.; Gaudart, J.; Magloire, R.; Raoult, D. Understanding the Cholera Epidemic, Haiti. *Emerg. Infect. Dis.* **2011**, *17*, 1161–1168.
4. Ministère de la Santé Publique et de la Population. Daily Reports of MSPP on the Evolution of Cholera in Haiti. Available online: http://www.mspp.gouv.ht/site/index.php?option=com_content&view=article&id=120&Itemid=1 (accessed on 30 December 2013).
5. Knox, R. Shots: NPR's Health Blog. Port-Au-Prince: A City Of Millions, With No Sewer System. Available online: http://www.npr.org/blogs/health/2012/04/13/150501695/port-au-prince-a-city-of-millions-with-no-sewer-system?ps=sh_sthdl (accessed on 2 May 2012).
6. Pan American Health Organization. Interactive Atlas of the Cholera Outbreak in La Hispaniola, 2010–2013. Available online: http://new.paho.org/hq/images/Atlas_IHR/CholeraHispaniola/atlas.html (accessed on 28 December 2013).
7. Codeço, C.T. Endemic and epidemic dynamics of cholera: The role of the aquatic reservoir. *BMC Infect. Dis.* **2001**, *1*, 1–14.

8. Tien, J.H.; Earn, D.J. Multiple Transmission Pathways and Disease Dynamics in a Waterborne Pathogen Model. *Bull. Math. Biol.* **2010**, *72*, 1506–1533.
9. Andrews, J.R.; Basu, S. Transmission dynamics and control of cholera in Haiti: An epidemic model. *Lancet* **2011**, *377*, 1248–1255.
10. Bertuzzo, E.; Mari, L.; Righetto, L.; Gatto, M.; Casagrandi, R.; Blokesch, M.; Rodriguez-Iturbe, I.; Rinaldo, A. Prediction of the spatial evolution and effects of control measures for the unfolding Haiti cholera outbreak. *Geophys. Res. Lett.* **2011**, *38*, L06403.
11. Tuite, A.R.; Tien, J.; Eisenberg, M.; Earn, D.J.; Ma, J.; Fisman, D.N. Cholera Epidemic in Haiti, 2010: Using a Transmission Model to Explain Spatial Spread of Disease and Identify Optimal Control Interventions. *Ann. Internal Med.* **2011**, *154*, 593–601.
12. Chao, D.L.; Halloran, M.E.; Longini, I.M., Jr. Vaccination strategies for epidemic cholera in Haiti with implications for the developing world. *Proc. Natl. Acad. Sci. USA* **2011**, *108*, 7081–7085.
13. Reiner, R.C., Jr.; King, A.A.; Emch, M.; Yunus, M.; Faruque, A.S.G.; Pascual, M. Highly localized sensitivity to climate forcing drives endemic cholera in a megacity. *Proc. Natl. Acad. Sci. USA* **2012**, *109*, 2033–2036.
14. Rinaldo, A.; Bertuzzo, E.; Mari, L.; Righetto, L.; Blokesch, M.; Gatto, M.; Casagrandi, R.; Murray, M.; Vesenbeckh, S.M.; Rodriguez-Iturbe, I. Reassessment of the 2010–2011 Haiti cholera outbreak and rainfall-driven multiseason projections. *Proc. Natl. Acad. Sci. USA* **2012**, *109*, 6602–6607.
15. Eisenberg, M.C.; Kujbida, G.; Tuite, A.R.; Fisman, D.N.; Tien, J.H. Examining rainfall and cholera dynamics in Haiti using statistical and dynamic modeling approaches. *Epidemics* **2013**, *5*, 197–207.
16. Knox, R. Shots: NPR's Health Blog. Vaccination Against Cholera Finally Begins in Haiti. Available online: http://www.npr.org/blogs/health/2012/04/12/150493770/vaccination-against-cholera-finally-begins-in-Haiti?ps=sh_sthdl (accessed on 2 May 2012).
17. United Nations. Haiti|ReliefWeb. Available online: http://reliefweb.int/country/hti (accessed on 10 January 2012).
18. Reyburn, R.; Kim, D.R.; Emch, A.; Khatib, A.; von Seidlein, L.; Ali, M. Climate Variability and the Outbreaks of Cholera in Zanzibar, East Africa: A Time Series Analysis. *Am. J. Trop. Med. Hyg.* **2011**, *84*, 862–869.
19. De Magny, G.C.; Murtugudde, R.; Sapiano, M.R.P.; Nizam, A.; Brown, C.W.; Busalacchi, A.J.; Yunus, M.; Nair, G.B.; Gil, A.I.; Lanata, C.F.; *et al*. Environmental signatures associated with cholera epidemics. *Proc. Natl. Acad. Sci. USA* **2008**, *105*, 17676–17681.
20. Koelle, K.; Rodó, X.; Pascual, M.; Yunus, M.; Mostafa, G. Refractory periods and climate forcing in cholera dynamics. *Nature* **2005**, *436*, 696–700.
21. Neilan, R.L.M.; Schaefer, E.; Gaff, H.; Fister, K.R.; Lenhart, S. Modeling optimal intervention strategies for cholera. *Bull. Math. Biol.* **2010**, *72*, 2004–2018.
22. Hartley, D.M.; Morris, J.G., Jr.; Smith, D.L. Hyperinfectivity: A critical element in the ability of *V. cholerae* to cause epidemics? *PLoS Med.* **2006**, *3*, e7:63–e7:69.

23. Huq, A.; Small, E.B.; West, P.A.; Huq, M.I.; Rahman, R.; Colwell, R.R. Ecological Relantionships Between *Vibrio cholerae* and Planktonic Crustacean Copepods. *Appl. Environ. Microbiol.* **1983**, *45*, 275–283.
24. Fotedar., R. Vector potential of houseflies (*Musca domestica*) in the transmission of *Vibrio cholerae* in India. *Acta Tropica* **2001**, *78*, 31–34.
25. Charles, R.C.; Ryan, M.E.T. Cholera in the 21st century. *Curr. Opin. Infect. Dis.* **2011**, *24*, 472–477.
26. NASA. NASA Earth Data. Daily TRMM and Other Satellites Precipitation Product (3B42 V7 derived) (TRMM_3B42_daily) [data files]. Available online: http://mirador.gsfc.nasa.gov/cgi-bin/mirador/ (accessed on 30 December 2013).
27. The Weather Underground. Mean Temperature (and Other) Weather History for Port-Au-Prince, Haiti. Available online: http://www.wunderground.com/history/airport/MTPP/2012/1/1/CustomHistory.html (accessed on 11 June 2012).
28. NOAA. NOAA Tides & Currents Website: Tide Predictions-Application. Available online: http://tidesandcurrents.noaa.gov/noaatidepredictions/NOAATidesFacade.jsp?Stationid=TEC4709 (accessed on 29 December 2013).
29. Banks, H.; Ernstberger, S.; Grove, S. Standard errors and confidence intervals in inverse problems: Sensitivity and associated pitfalls. *J. Inv. Ill-Posed Probl.* **2006**, *15*, 1–18.
30. Ramsay, J.; Hooker, G.; Campbell, D.; Cao, J. Parameter estimation for differential equations: A generalized smoothing approach. *J. R. Stat. Soc.: Ser. B (Stat. Methodol.)* **2007**, *69*, 741–796.
31. Kaper, J.B.; Morris, J.G., Jr.; Levine, M.M. Cholera. *Clin. Microbiol. Rev.* **1995**, *8*, 48–86.
32. Fung, I.C.H. Cholera transmission dynamic models for public health practitioners. *Emerg. Themes Epidemiol.* **2014**, *11*, 1–11.
33. Legros, D.; Paquet, C.; Perea, W.; Marty, I.; Mugisha, N.K.; Royer, H.; Neira, M.; Ivanoff, B. Mass vaccination with a two-dose oral cholera vaccine in a refugee camp. *Bull. World Health Org.* **1999**, *77*, 837–842.
34. CIA. CIA The World Factbook 2013–2014. Available online: https://www.cia.gov/library/publications/the-world-factbook/index.html (accessed on 25 January 2014).
35. Date, K.A.; Vicari, A.; Hyde, T.; Mintz, E.; Danovaro-Holliday, M.C.; Henry, A.; Tappero, J.W.; Roels, T.H.; Abrams, J.; Burkholder, B.T.; *et al*. Considerations for oral cholera vaccine use during outbreak after earthquake in Haiti, 2010–2011. *Emerg. Infect. Dis.* **2011**, *17*, 2105–2112.
36. CERF (Office for the Coordination of Humanitarian Affairs-United Nations). CERF Gives $8 Million to Support Humanitarian Activities in Haiti. Available online: http://ochaonline.un.org/CERFaroundtheWorld/Haiti2012/tabid/7810/language/en-US/Default.aspx (accessed on 10 July 2012).